DEPARTMENT OF DEFENCE
DEFENCE SCIENCE & TECHNOLOGY ORGANISATION
DSTO

DSTO

# An Analytically Validated Highly Damped Repair for Acoustically - Induced Cracking on the F/A-18 Nacelle Skin

S.C Galea and R.J.Callinan

DSTO-TR-1162

# An Analytically Validated Highly Damped Repair for Acoustically - Induced Cracking on the F/A-18 Nacelle Skin

*S. C. Galea and R. J. Callinan*

**Airframes and Engines Division**
**Aeronautical and Maritime Research Laboratory**

DSTO-TR-1162

## ABSTRACT

The skin of an aircraft can vibrate as a result of pressure waves caused by engine and/or aerodynamic effects. In modern fighter aircraft such as the F/A-18, overall sound pressure levels have been recorded up to 170 dB over the surface of the skin. In the F/A-18, cracking has occurred in the lower nacelle external skin, typically along the boundaries of the panel. These cracks often originate from a fastener line and grow along the boundary and then turn into the centre of the panel. In the case of the F/A-18, cracking was due to higher than expected pressure levels caused by an aerodynamic disturbance at the inlet lip. Initial design of this region was based on an overall sound pressure of 160db, which was based on initial computational fluid dynamics (CFD) work. An attempt was made to repair a panel with a boron fibre patch however this repair did not appear to significantly reduce the crack growth. The design of the repair was based on in-plane loads only. In this report the aim is to develop a patch design, based on a finite element analysis, which significantly reduces crack stress intensity factor for structures subject to intense acoustic environments. A significant reduction in stress intensity is achieved by using a highly-damped patch which incorporates a uni-directional boron/epoxy repair and constrained damping layers which consists of viscoelastic material, which provides the necessary damping, and [0/90] boron/epoxy constraining layers. Such configurations have shown that theoretical reductions in stress intensity factors of up to 10 times are achievable. This has the potential of reducing the mode I stress intensity factor ($K_I$ ) to the order of $K_I$ threshold thus substantially reducing crack growth.

*Published by*

*DSTO Aeronautical and Maritime Research Laboratory*
*506 Lorimer St*
*Fishermans Bend Vic 3207 Australia*

*Telephone: (03) 9626 7000*
*Fax: (03) 9626 7999*

*AR-011-893*
*June 2001*

**APPROVED FOR PUBLIC RELEASE**

# An Analytically Validated Highly Damped Repair for Acoustically - Induced Cracking on the F/A-18 Nacelle Skin

## Executive Summary

Acoustic fatigue is fatigue of the structure resulting from exposure to high intensity noise caused by either propulsion, rotor or aerodynamic sources. Acoustically-induced cracking (also termed high cycle fatigue) has occurred on the external surface of the lower nacelle skin on the F/A-18. In these regions overall sound pressure levels (OASPL) greater than 170 dB have been measured in flight. These high sound pressure levels appear to be a result of an aerodynamic disturbance at the nacelle inlet lip. Typical cracks occur on the longer side of the panel, along a line of rivets or run parallel to the rivet line and may turn into the centre of the panel. Up to a third of the F/A-18's in the RAAF fleet are affected by these cracks.

The standard long term fix is to incorporate additional aluminium stiffeners on the inside to stiffen the panel. This has two effects; firstly to reduce the panels response, i.e. lower stress, for a given load and secondly it increases the resonant frequencies of the panel to frequencies well outside the excitation frequencies. Composite bonded repairs can be an attractive alternative to the current mechanical fix since the manafacture and implementation of the former takes between 15-25 hours compared to 60 hours for a mechanical repair. Attempts have been made to repair these panels with boron/epoxy fibre patches, however the cracks have continued to grow at what appears to be an unchanged rate. However these repairs were designed for the static in-plane load case and neglected the high frequency out-of-plane excitation. In this report new concepts of patch design are established in order to repair cracked structures subjected to out-of-plane high frequency excitation. The report shows that the addition of damping material to a bonded repair (referred to here as a highly damped-patch) can result in sigificant reductions in crack growth rate. The study involves the estimation of the root mean square (rms) stress intensity factor ($K$) in the cracked and cracked/repaired cases. Finally it is theoretically verified that the highly-damped patch can significantly reduce crack growth and therefore yield acceptable crack lengths for a 6000 hour lifetime condition.

# Authors

**S. C. Galea**
Airframes and Engines Division

*Dr Galea graduated in 1980 with a Bachelor of Engineering (Mech) from the University of Queensland with first class honours and in 1983, he received a Masters of Engineering Science. He commenced employment with the Aeronautical Research Laboratory in 1983. In 1985 he commenced studies at the Institute of Sound and Vibration Research, University of Southampton, UK and received his Doctor of Philosophy from the University of Southampton in 1989. Dr Galea was appointed a Research Scientist in 1990 and Senior Research Scientist in 1992. Since 1990 Dr Galea has been working in the areas of composite structures, computational and experimental mechanics. He is currently managing the smart materials/structures for airframes task, at the Aeronautical and Maritime Research Laboratory. His other areas of research include bolted and bonded composite joints, repairs to acoustically-induced cracked structures and structural health monitoring.*

**R. J. Callinan**
Airframes and Engines Division

*Mr. R.J.Callinan is a senior research scientist and graduated from RMIT (Aero. Eng.) in 1969 and from Monash University in 1971 (Civil. Eng.) and completed a M.Eng. Sc. in 1981 at Melbourne University. His work has been in the areas of finite element analysis, fracture mechanics and structural mechanics of composite and bonded repairs, military aircraft accident investigations. He has also been involved with design studies of low radar cross-section battlefield surveillance R.P.V.'s. In 1985 he was seconded to the USAF at Eglin AFB for 18 months, to carry out vulnerability studies on composite structures. More recently he has been involved in a specific program on validation of bonded repairs to RAAF aicracft, and bonded repairs subject to acoustic fatigue.*

# Contents


1. INTRODUCTION ..... 1

2. CRACKING HISTORY AND FRACTOGRAPHIC ANALYSIS ..... 2

3. ANALYSIS OF PANELS SUBJECT TO ACOUSTIC EXCITATION ..... 5
3.1 Random response analysis ..... 5
3.2 FEA Methodology validation ..... 6
3.3 Stress intensity factors ..... 8
3.4 Power spectral density of the excitation ..... 9
3.5 Strain gauge data ..... 10

4. CRACKED PANELS - UNREPAIRED AND REPAIRED USING EXISTING TECHNIQUES (C5033) ..... 12
4.1 FEA of cracked nacelle inlet ..... 12
4.2 Crack growth study ..... 13
4.3 Summary of repair failure investigation ..... 22

5. HIGHLY DAMPED REPAIRS FOR CRACKED PANELS ..... 23
5.1 Design of highly damped patch ..... 23
5.2 Damping of highly damped patch ..... 23
5.3 Results for unrepaired cracked plate ..... 27
5.4 Analysis of highly damped repair to a cracked plate ..... 28
5.5 Results and Discussion ..... 28
5.5.1 Modal shapes and frequencies ..... 29
5.5.2 PSD of the displacement. ..... 30
5.5.3 Stress intensity factor. ..... 31
5.5.4 Crack growth predictions. ..... 32

6. CONCLUSIONS ..... 35

7. ACKNOWLEDGMENTS ..... 35

8. REFERENCES ..... 36

# Notation

| | |
|---|---|
| $E$ | Young's modulus |
| $E_{al}$ | Young's modulus for aluminium |
| $E_r$ | Young's modulus for repair |
| $E_1$ | Young's modulus for plate |
| $E_2$ | Young's modulus for reinforcement |
| $e$ | modal energy |
| $e_i$ | modal energy for $i$ th element |
| CLD | constrained layer damping |
| COD | crack opening displacement |
| G | shear modulus |
| $H(w)$ | transfer function |
| $K$ | rms stress intensity factor |
| $K_{IC}$ | fracture toughness |
| $(K_I)_{rms}$ | mode I rms stress intensity factor |
| $(K_{II})_{rms}$ | mode II rms stress intensity factor |
| $(K_{III})_{rms}$ | mode III rms stress intensity factor |
| [K] | stiffness matrix |
| $l$ | size of crack tip element |
| OASPL | overal sound pressure level |
| $p_I$ | excitation pressure |
| $p_{rms}$ | rms fluctuating pressure |
| PSD | power spectral density |
| $S_J$ | power spectral density of the response |
| $S_I$ | power spectral density of the excitation |
| SPL | sound pressure level |
| $J_{rms}$ | root mean square of the response |
| $t_{al}$ | thickness for aluminium |
| $t_r$ | thickness for repair |
| $u_J$ | displacement due to excitation pressure |
| $u_{rms}$ | mode I rms crack opening displacement |
| $v_{rms}$ | mode II rms crack opening displacement |
| $w_{rms}$ | mode III rms crack opening displacement |
| V | volume |
| VEM | visco-elastic material |
| $\delta$ | eigenvector |
| $\varpi$ | frequency |

| | |
|---|---|
| $\eta_S$ | structural loss factor |
| $\eta_i$ | material loss factor for $i$ th element |
| $\nu_{12}$ | poisson's ratio |

# 1. Introduction

Acoustic fatigue is due to a very high intensity excitation as a result of pressure waves caused by either engine or aerodynamic effects. Acoustically-induced cracking has occurred on the external surface of the lower nacelle skin on the F/A-18, as illustrated in Fig. 1. In these regions overall sound pressure levels greater than 170 dB have been measured in flight [1]. These high sound pressure levels appear to be a result of an aerodynamic disturbance at the inlet lip [1]. Typical cracks occur along a line of rivets or run parallel to the rivet line and may turn into the centre of the panel, as shown in the inset. Cracking generally occurs along the longer side of the panel where the bending stresses due to out-of-plane vibrations are a maximum. Up to a third of the F/A-18's in the RAAF fleet are affected by these cracks.

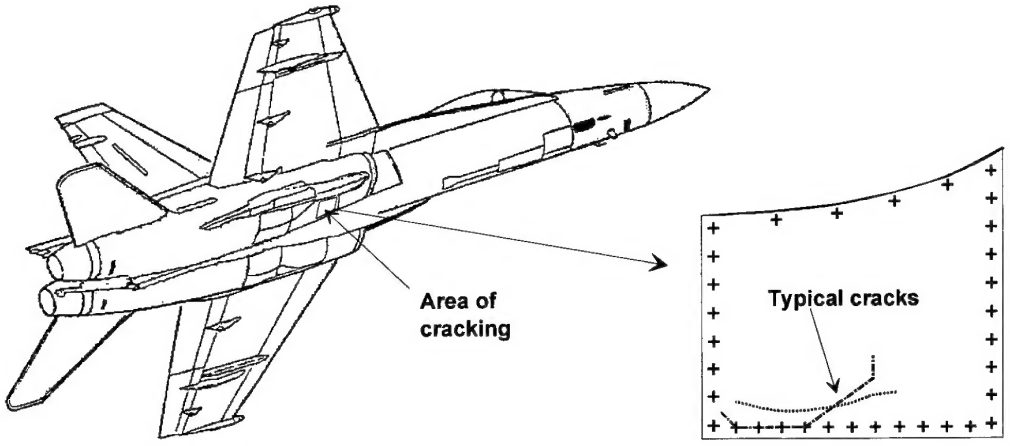


*Figure 1 - Location of the cracking in the lower nacelle inlet.*

The standard repair for such cracking is to remove and replace the panel. The standard long term fix is to incorporate additional stiffeners on the inside to stiffen the panel. This has two effects; firstly to reduce the panels response, i.e. lower stress for a given load and secondly it increases the resonant frequencies of the panel to frequencies well outside the recorded excitation frequencies.

In order to reduce the cost of repairing such cracked structures a bonded composite repair would be preferred. The benefits of such a repair are reflected in the time required to carry out the repair; typically 60 hours for the mechanical repair and approximately 15-25 hours for the bonded repair. Such a bonded repair was designed, based on a standard repair design procedure, and implemented on an existing cracked aircraft. While in the past boron fibre/epoxy resin patches have been extremely successful, in repairing cracked metallic secondary and primary structures [2], in this case significant crack growth occurred after the application of the repair. This unsuccessful application of a bonded repair to a cracked metallic structure was due to the fact that the standard design procedure [3] is based on in-plane low cycle (quasi-static) loading condition. However for the acoustic

environment a new design approach for bonded repairs is required, i.e. a design procedure based on dynamic out-of-plane high-cycle loading. Work carried out by Callinan et al [4, 5] showed that the addition of damping to a bonded repair can result in significant reductions of crack growth. These authors showed that a low-damping patch covering the entire panel resulted in a reduction of the mode $I$ stress intensity factor, $K_I$, from 18 MPa$\sqrt{m}$, for a cracked unrepaired panel, to 6 MPa$\sqrt{m}$. Although this is not a high value in comparison with the fracture toughness value, $K_{IC}$, ( 23-27MPa$\sqrt{m}$) in an environment of high-cycle fatigue it leads to a high crack growth rate. They found that by further increasing the damping of the repaired structure, from a loss factor of 0.032 to 0.128, reduced the stress intensity to 4 MPa$\sqrt{m}$. Work carried out by Rodgers et al [6] and Liguour et al [7] also indicates that the addition of damping can significantly reduce the crack growth rate.

This report firstly investigates the failure of the low damped boron/epoxy repair. Secondly the report details the design of a highly-damped bonded repair, incorporating constrained layered damping (CLD), using finite element analysis (FEA) of the structure subject to simulated acoustic loading conditions. CLD material incorporates a layer of visco-elastic material (VEM) with a constraining layer attached to the top of the VEM. The study involves the estimation of the root mean square (rms) stress intensity factor ($K$) in the cracked and cracked/repaired cases. Various patch design parameters, such as reinforcing patch dimensions, thicknesses of the (viscoelastic) damping material and thickness of the constraining layer are considered in order to maximise the effectiveness of the patch and thus lower the stress intensity. Finally it is theoretically verified that the highly-damped patch can significantly reduce crack growth and therefore yield acceptable crack lengths for a 6000 hour lifetime condition.

## 2. Cracking History and Fractographic Analysis

As a result of the failure of the boron/epoxy repair to prevent crack growth, the particular panel was removed from the aircraft for replacement and and assessment [8] of the fracture surface. The inside surface of a section of the cracked panel is shown in Fig. 2, and the missing section was that used for the examination. It was found that the crack had started on the inner surface, and at the edge of the panel which is thicker than the chemical mill section, and developed as a semi-elliptical surface crack, Fig. 3, until it became deep enough to penetrate the thickness of the panel. The crack proceeded as a through crack, with crack fronts being inclined as shown in Figs. 4 and 5 corresponding to a final crack length of 135mm. The central region of the crack just before the boron/epoxy repair was applied is shown in Fig. 6 and indicates rubbing of the crack faces due to transverse movement. This would correspond to a mode III crack tip driving force. However after the patch was applied a change in crack growth mode occurred. This is seen in Figs. 4 and 5 where the crack is bright and highly detailed in comparison to that shown in Fig. 6. After the repair the shape of the crack front indicates that bending was involved. This is consistent with a neutral axis offset caused by the bending of both the boron/epoxy and panel in which the maximum stress occurred in the inner surface of the panel.

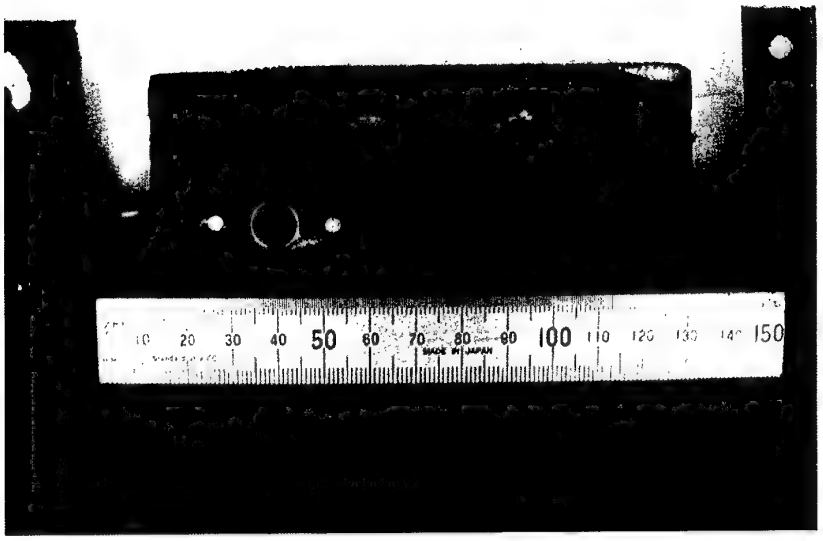


*Figure 2. The panel from which the small piece was removed [8].*

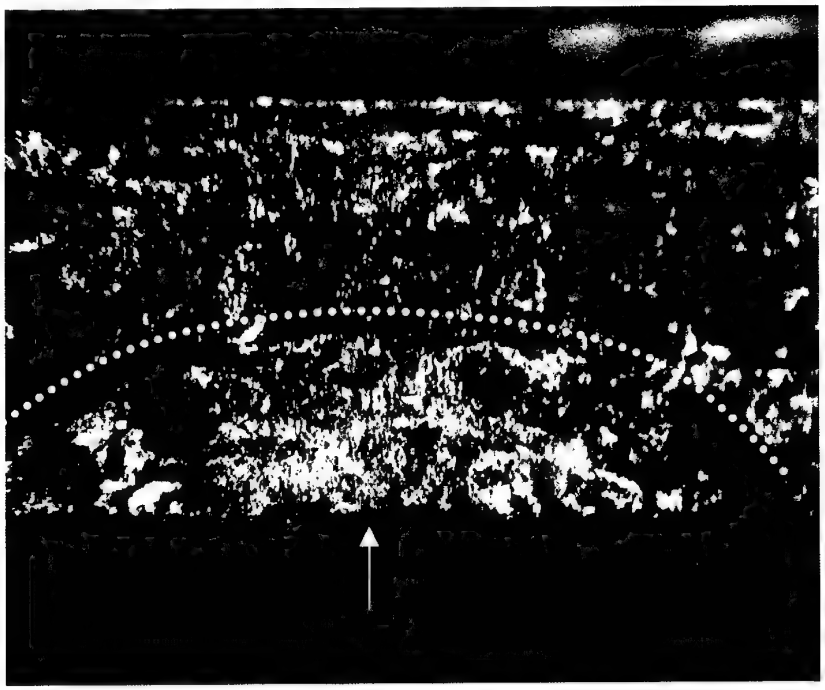

*Figure 3. The origin of the crack in the panel (arrowed). The remains of the semi-elliptical surface crack can be seen just below the dotted line. This crack was located on the inside surface of the thicker section of panel. Note the smooth rubbed character of the surface, indicating large relative motions between the two halves of the crack [8].*

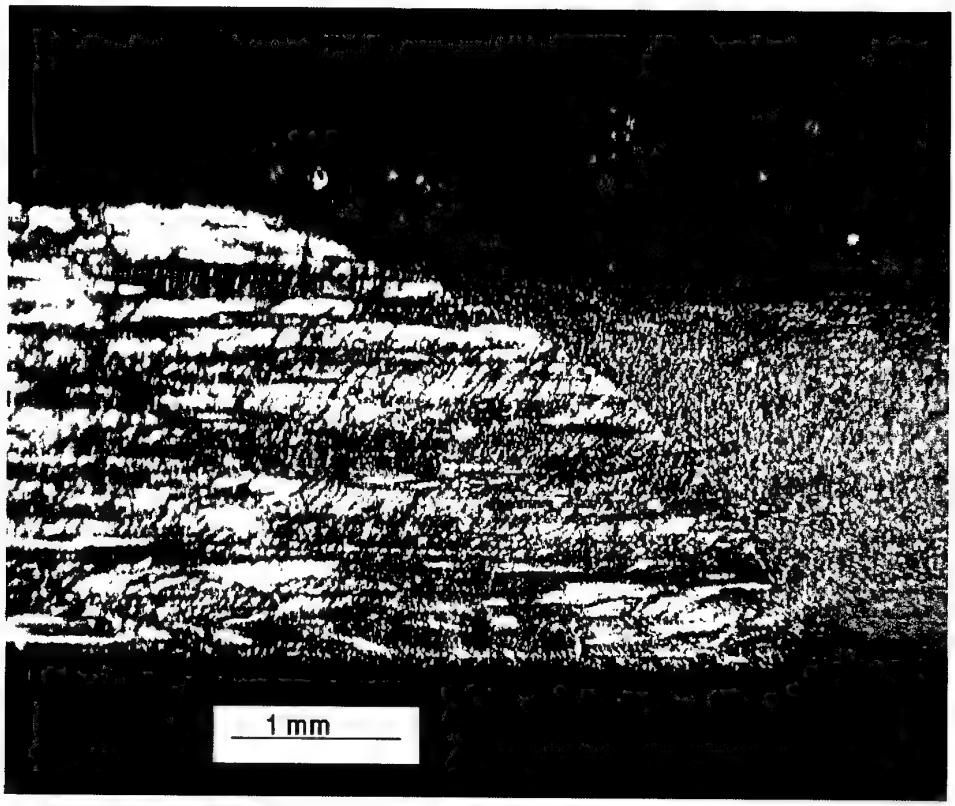


*Figure 4. View of the tip of the crack in the thick end of the panel. The fatigue crack surface is the bright faceted region to the left and the deliberately broken surface is the mottled grey area to the right. Note the shape of the crack, much longer along the inside surface of the panel, indicating that a degree of bending was involved in the development of the crack. Also note that the fatigue crack surface is bright and highly detailed, and does not appear to have been rubbing [8].*

*Figure 5. View of the tip of the crack in the thinner part of the panel. The same comments as above for Figure 4 apply [8].*

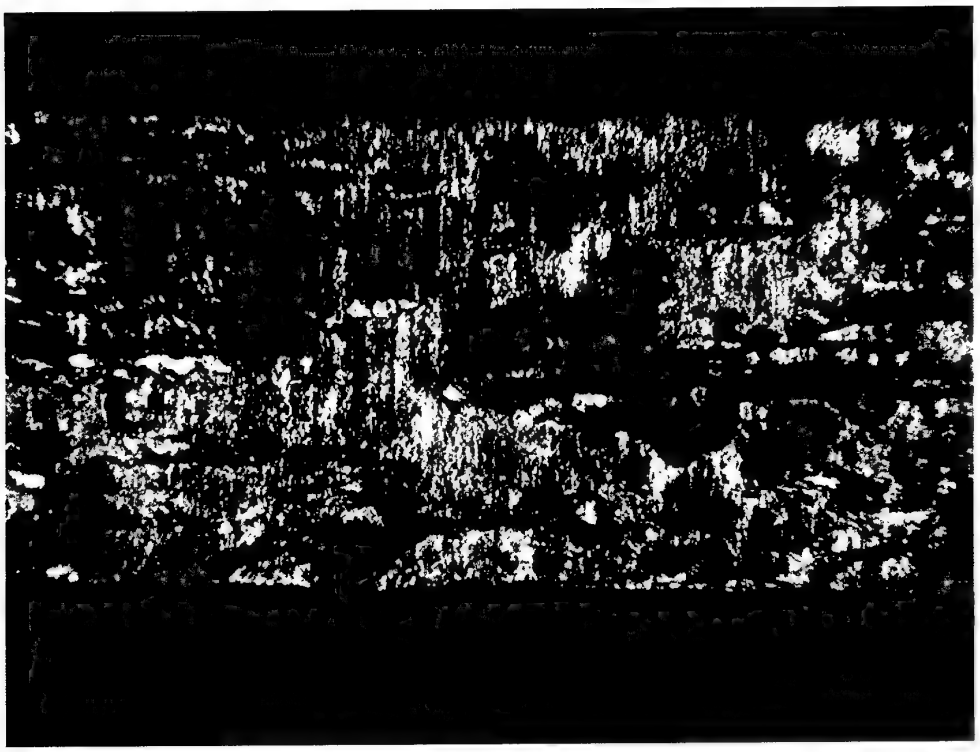

*Figure 6. View of the central area of the crack, showing the presence of pronounced rubbing [8].*

Both the length of the crack tip after the repair and flight hours are known for the right hand crack tip shown in Fig. 2, and is 2 mm/flight hour. While the crack growth rate before the repair is unknown it is thought to be considerably less than that after the repair. There is a possibility that before the repair, the rubbing of the crack faces provided some friction damping to the panel, this in turn led to a lower crack growth rate.

# 3. Analysis of Panels Subject to Acoustic Excitation

## 3.1 Random Response Analysis

NASTRAN [9] has been used to predict the random response of a panel (cracked or uncracked) subject to acoustic excitation. The system response to random excitation is evaluated via the frequency response technique viz.,

$$S_J(\omega) = |H(\omega)|^2 S_I(\omega) \qquad (1)$$

where in this case $H(\omega)$ is the frequency response of a displacement $u_J$ due to an excitation force (pressure) $p_I$. $S_J$ and $S_I$ are the Power Spectral Density (PSD) of the response (displacement) and of the excitation (pressure), respectively.

This analysis allows the statistical properties of the system to be evaluated. Random vibrations considered here involve all frequencies at any one instant in time. After calculating the PSD, the root mean square (rms) of the response can be determined by computing the square root of the PSD area:

$$j_{rms} = \sqrt{\frac{1}{2\pi}\int_0^\infty S_j(\omega)\, d\omega} \tag{2}$$

where the limits of the integral will be truncated as specified by the excitation spectrum. No structural response is expected below 30 *Hz* and the excitation levels above 8000 *Hz* are minimal.

A similar application of finite element techniques to undertake a PSD analysis to acoustic fatigue problems has been reviewed by Climent and Casalengua [10].

## 3.2 FEA Methodology Validation

The complexity of the random response analysis and number of assumptions made was such that validation of the analysis was necessary. Both experimental and analytical work has been carried out by Byrnes [11]. In this case the plate used is that shown in Fig. 7 and the PSD of the acoustic excitation is given in Fig. 8. Dimensions of the plate are *B=500 mm*, *C=166 mm* and thickness=*1.2 mm* with a crack of length A. This plate was clamped along all of the edges except one edge, which was partially restrained. The unrestrained region represented a crack along one side. The length of the crack has been expressed as a ratio A/B. Material properties of the aluminium plate are given in Table 2, with the loss factor set to 0.0275. R.m.s. strains were measured at a point 25 mm ahead of the crack tip, the results are reproduced in Fig. 9 along with an analytical solution also developed by Byrnes [11].

The F.E. results are also shown in Fig. 9. Only three experimental data points were published in [11], and in each case the F.E. results are within 10%. However disagreement does exist with the analytical solution for crack length to plate width ratios below 0.4 . It is not clear why this difference occurs. The analytical solution is based on contributions from the first and second mode shapes only. However, the F.E. PSD of the response includes all the structural modes between 30-8000 *Hz*.

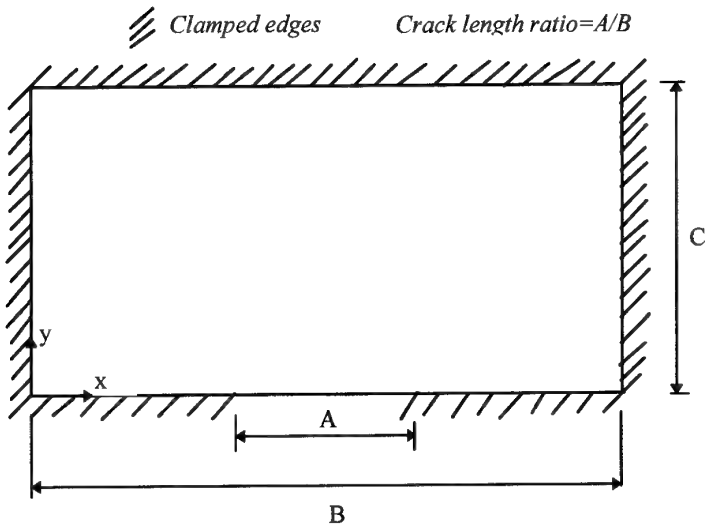


*Figure. 7: Geometry of plate used for the validation of the analysis.*

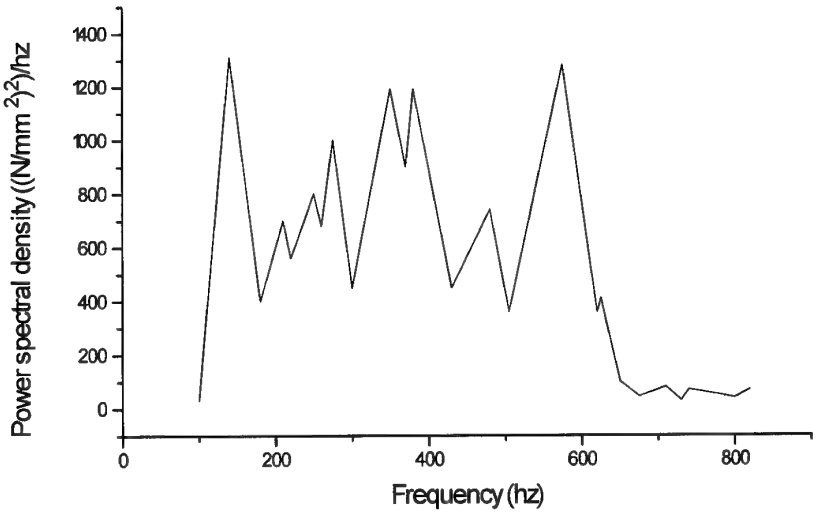


*Figure. 8: Power Spectral Density of the pressure excitation used in [11].*

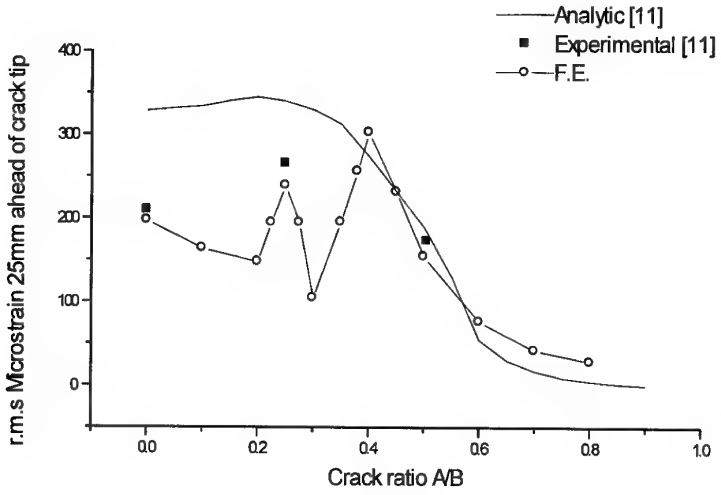


*Figure. 9: Comparison of F.E., experimental and analytic results.*

## 3.3 Stress Intensity Factors

In the F.E. model the depth of the plate is modelled using a single layer of 20 noded brick elements, which allows the model to account for the bending behaviour of the skin. The skin thickness is approximately 1 mm, hence the condition of plane stress is assumed. The computation of the stress intensity factor may be determined directly from the crack tip element used around the crack tip or from displacements using a crack opening (COD) formula. The rms crack tip stress intensity factors for mode *I*, *II* and *III* are derived from the standard asymptotic relations:

$$K_{I\,rms} = \frac{Eu_{rms}}{4}\sqrt{\frac{2\pi}{l}} \tag{3}$$

$$K_{II\,rms} = \frac{Ev_{rms}}{4}\sqrt{\frac{2\pi}{l}} \tag{4}$$

$$K_{III\,rms} = Gw_{rms}\sqrt{\frac{2\pi}{l}} \tag{5}$$

where

$E$ = Young's modulus,

$G$ = Shear modulus

$u_{rms}$ = mode *I* crack opening rms displacement (i.e. displacement out-of-plane of crack )

$v_{rms}$ = mode *II* crack opening rms displacement (i.e. displacement in-plane, parallel to plane of crack )

$w_{rms}$ = mode *III* crack opening rms displacement (i.e. displacement in-plane, transverse to plane of crack )

$l$ = length of the crack tip element

## 3.4 Power Spectral Density of the Excitation

One third octave sound pressure level (SPL) measurements [1], have been made in flight using microphones located at the nacelle inlet area, and are shown in Fig. 10 with increasing frequency. The spectrum level, relative to the overall sound pressure level (OASPL) of 170*dB*, was derived from these data and is also shown in Fig. 10. This spectrum is now used to calculate $S_1$.

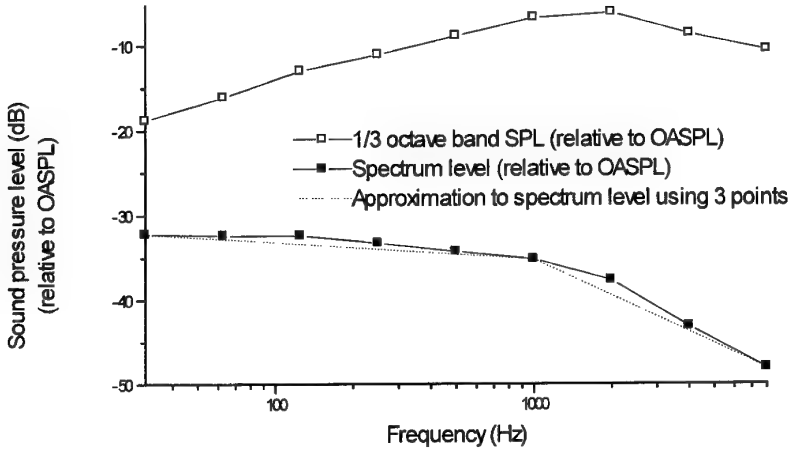


*Figure 10. Spectrum and one-third octave band levels of sound pressure over nacelle inlet.(OASPL=170dB)*

The relationship between the SPL and the r.m.s. fluctuating pressure (p) is given in [6] as:

$$p_{rms} = 10^{(SPL/20-4.69897)} \tag{6}$$

and the power spectral density of acoustic pressure, i.e. PSD of the excitation, at any given frequency is given by:

$$PSD = p_{rms}{}^2 = 10^{(SPL/10-9.3979)} \tag{7}$$

The curve in Fig. 10 has been approximated by two straight lines defined by the three points shown in Table 2. This approximate spectrum is used as the excitation PSD.

*Table 1: Input power spectral density*

| Frequency (Hz) | Pressure spectrum level (dB) | PSD $(MPa)^2/Hz$ |
|---|---|---|
| 31.5 | 140 | $4.0 \times 10^{-8}$ |
| 1000 | 137 | $2.005 \times 10^{-8}$ |
| 8000 | 124.1 | $1.028 \times 10^{-9}$ |

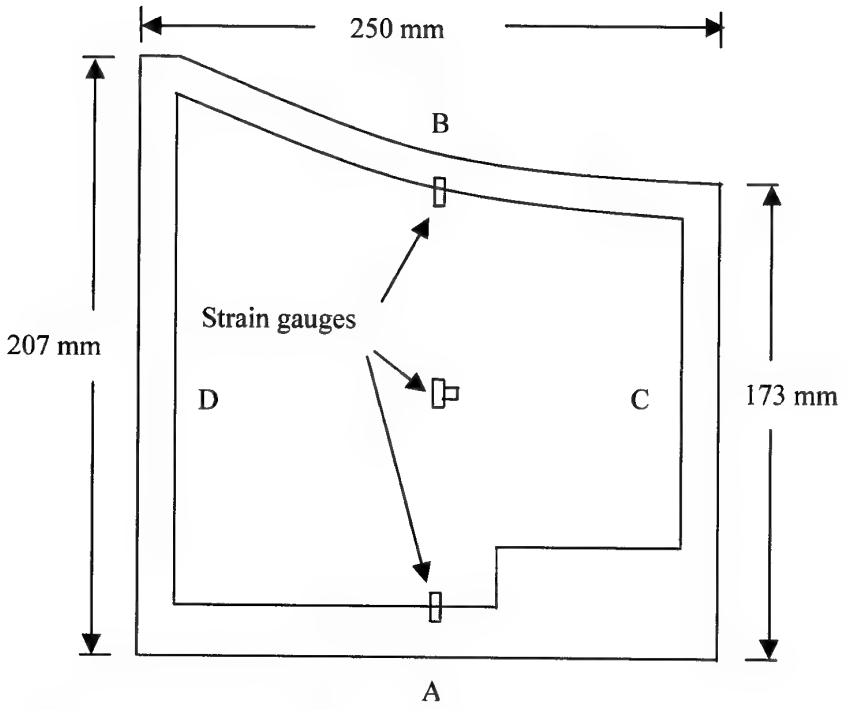


*Figure 11. Location of strain gauges on right hand nacelle panel [1].*

## 3.5 Strain Gauge Data

Strain gauge flight data have been obtained for the F/A-18, [1], using single gauges on the edge of the panel and a strain gauge rosette shown in Fig. 11. Specifically these locations correspond to regions of high strain. A finite element model representing the double curvature of the skin panel was developed corresponding to the outline shown in Fig. 11. This model was calibrated by adjusting the curvature such that very close results were obtained for the first three mode shapes and frequencies. The power spectral density defined in Table 1 was used as the excitation condition in this case.

The *rms* strain results shown in Fig. 12 represent a traverse on the outside skin from point A to B, while in Fig. 13 the results correspond to a traverse from point C to D. The high strain gradients at the edge of the panel are due to the step change in panel thickness due to chemical milling. As such it is difficult to assess the accuracy of these results except that the F.E. analysis appears to be conservative. The complexity of this F.E. model was such that to carry out parametric analysis was very time consuming and as a result flat panel models were considered instead.

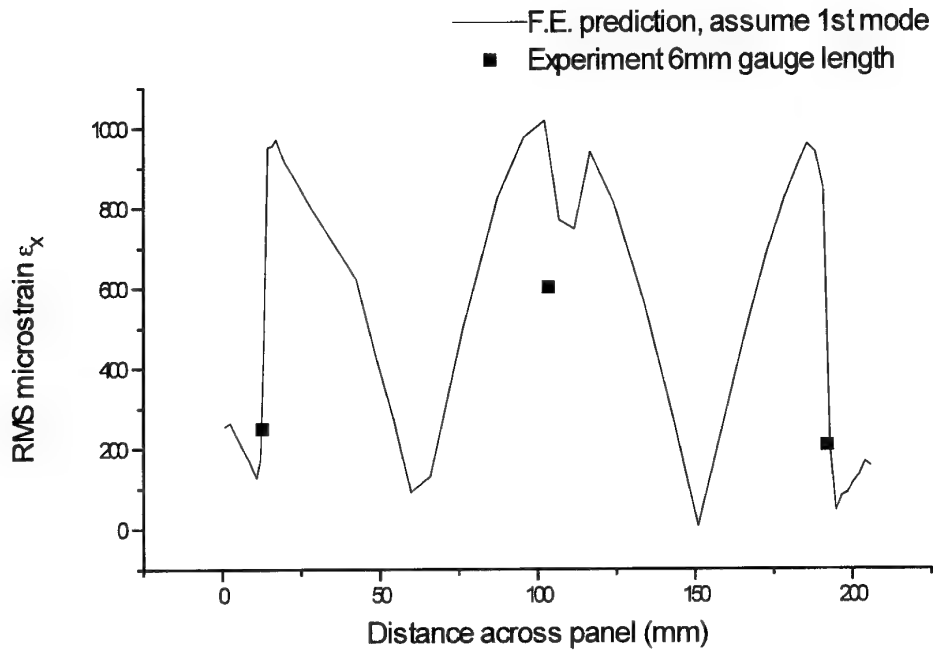


*Figure 12. Strain distribution along line from points A to B, see Figure 11.*

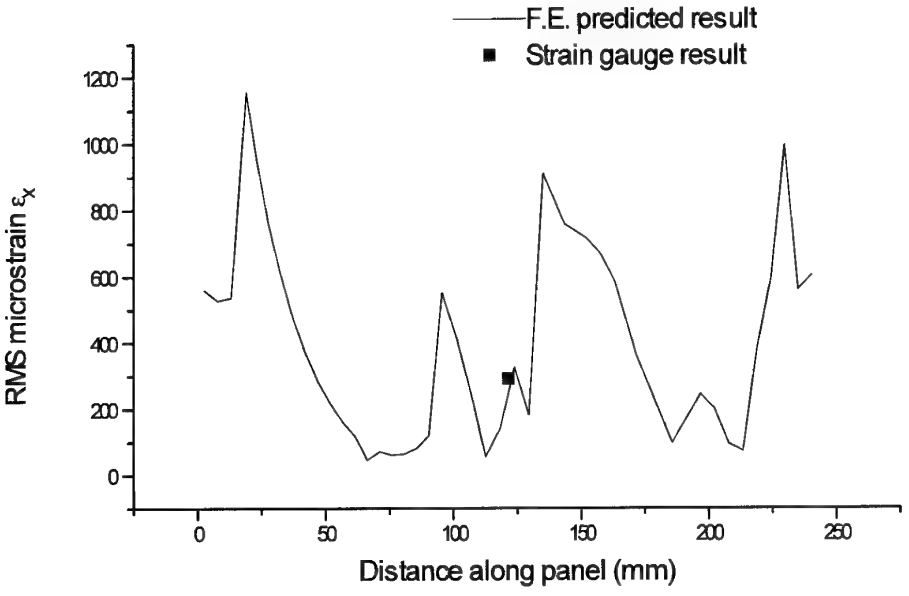


*Figure 13. Strain distribution along line from points C to D, see Figure 11.*

# 4. Cracked Panels - Unrepaired and Repaired Using Existing Techniques (C5033)

The work carried out in this section is based on [4] and shows the expected performance of a low damped patch designed to RAAF Engineering Standard C5033, [3]. This section evaluates the stress intensity factors for the unpatched and the patched configuration.

## 4.1 FEA of Cracked Nacelle Inlet

In order to study the cracking mechanisms of the cracked and cracked/repaired nacelle skin cases, a simplified model has been developed in which the skin is considered to be a flat rectangle. However, to take account of all shear deformation the structure has been idealised as a fully three-dimensional structure using 20 noded brick elements. The geometry of the structure is shown in Fig. 14. The mesh size of the skin structure is 75x60 elements, while the patch and skin is 40x40 elements. As shown, the uni-directional patch only extends partially across the panel. It also covers an adjacent panel as shown in the dotted outline. Sufficient elements have been used to define the minimum crack length considered. Material properties for the skin, adhesive and boron are shown in Table 2. The Young's modulus of the composite in the $0^0$ fibre direction is $E_1$ , and $E_2$ in the transverse direction. The main reason that 20 noded bricks were used in the skin is that calculations for $K$ can be made corresponding to a bending field. Also, the behaviour of the adhesive has been modelled as a 3 dimensional element, to allow for shear deformation. A loss factor of 0.016 has been used [1].

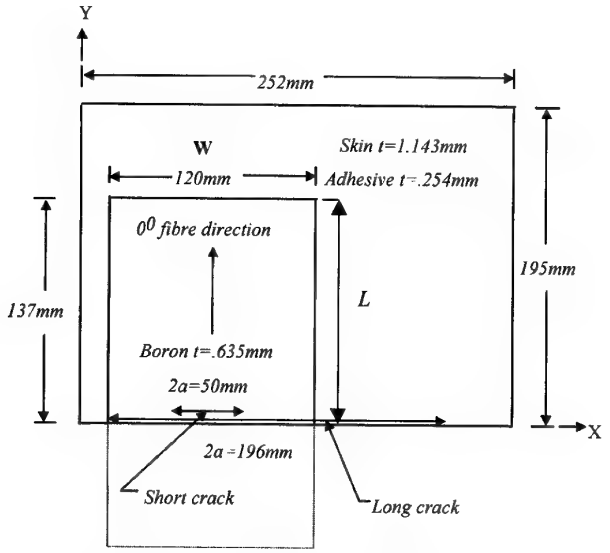


*Figure 14: Dimensions of simplified F/A-18 nacelle inlet panel, with crack and patch.*

The boundary conditions for this model are considered to be fully clamped except for the crack region which is not restrained. The patch above the crack also remains fully constrained. Clearly crack closure will occur at an increasing distance away from the crack tip, however the complexity in introducing such constraints has not been included in this preliminary study. The crack is initially 50*mm* long with it's centre located within the patch. A number of crack lengths have been considered to simulate the crack growth. The crack is assumed to grow symmetrically until the left hand crack tip extends to the edge of the patch. At this point no more crack growth occurs due to the proximity of the panel boundary. The only growth that occurs is at the right hand crack tip. In this study the maximum crack length considered is 196*mm*.

*Table 2- Material properties used in the FEA.*

| Material | Young's modulus (MPa) | Ratio of Young's modulus ($E_1/E_2$) | Poisson's ratio ($\nu_{12}$) | Shear modulus (MPa) | Density ($x10^{-9}$ $Mg/mm^3$) |
|---|---|---|---|---|---|
| Aluminium | 71000. | 1. | 0.33 | 26691. | 2.77 |
| Adhesive | 2273. | 1. | 0.35 | 842. | 1.2 |
| Boron | 207000. | 10.89 | 0.21 | 4800. | 2.0 |
| VEM (20°C) | 5700. | 1. | 0.30 | 2192. | 1.75 |

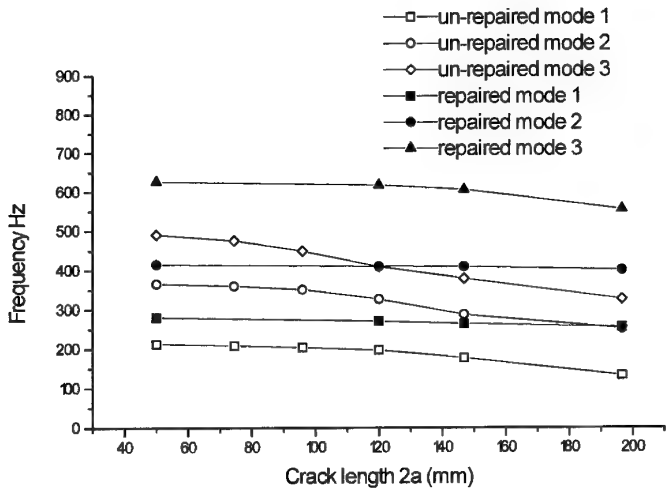


*Figure 15. Frequency versus crack length for un-repaired and repaired cases.*

## 4.2 Crack Growth Study

Shown in Fig. 15 are the natural frequencies versus crack length for the cracked un-repaired panel and also the cracked repaired panel for the first 3 resonant modes. In the case of the cracked un-repaired structure, increasing the crack length significantly reduces

the resonant frequencies of the panel. Also as expected, repaired panels have little variation in natural frequencies with crack length. Furthermore, the repaired panels have substantially higher natural frequencies for all modes than the un-repaired panels. The boron repair has a definite influence on the panel stiffness.

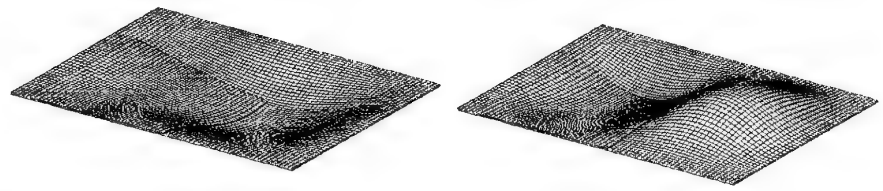

Mode 1, 280.3 Hz Mode 2, 414.9 Hz

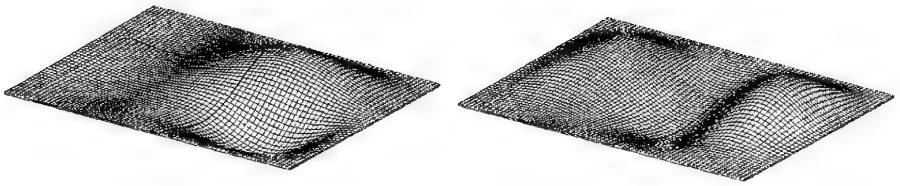

Mode 3, 626.5 Hz Mode 4, 687.8 Hz

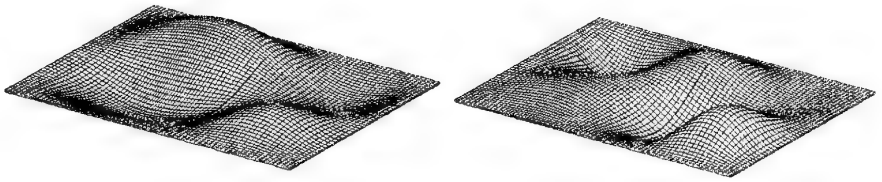

Mode 5, 817.0 Hz Mode 6, 1021.1 Hz

*Figure 16. Mode shapes for the repaired panel containing a short crack (2a = 50mm).*

Mode shapes have been computed corresponding to a short and long crack length for the repaired panel. The first 6 mode shapes for a repaired panel containing a short, *50 mm* crack, are shown in Fig. 16. Clearly the mode shapes in Fig. 16 indicate that the crack tip behaviour is dominated by the mode *I* stress intensity factor $K_I$. This is shown by the bending in the region of the crack. Fig. 17 shows the mode shapes of a repaired panel where the long, *196 mm*, crack now extends outside the patch (see Fig. 14). These mode shapes indicate that the unsupported crack tip behaviour will now have significant contributions from mode *III* stress intensity factor, $K_{III}$.

The rms mode *I* stress intensity factor $(K_I)_{rms}$ for the cracked un-repaired panel is shown in Fig. 18a. As expected, the general response is an increase of $(K_I)_{rms}$ with crack length. The

left hand crack tip is always closer to the clamped edge of the panel than the right hand crack tip, and since the bending stresses are a maximum midway along the boundary, the right hand tip gives the highest value of $(K_I)_{rms}$. The values of $(K_I)_{rms}$ in relation to the fracture toughness, are significant and explain crack growth. For crack growth, threshold values of $(K_I)_{rms}$ are shown in Fig. 31.

In the repaired panel the neutral axis is offset and as a result $(K_I)_{rms}$ is evaluated at both inner and outer surfaces of the skin; the repair being applied to the outer surface. Being a one sided repair the repair is more effective on the outer surface which is more closely restrained [6]. These bending effects are clearly shown in Fig. 18b. The right hand crack results in the highest values for $(K_I)_{rms}$ located on the inner surface. These values of $(K_I)_{rms}$ are significantly high before the crack grows out from under the patch and explain continued crack growth. For a normal 'static' repair in which the only significant events are manoeuvre and gust loads, the repair would be successful. However, in the acoustic excitation environment, the resonant frequency of the actual nacelle panel is of the order of 300-400Hz thus causing the repair to be ineffective.

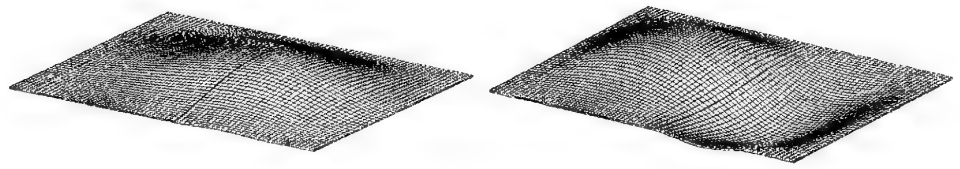

Mode 1, 255.1 Hz

Mode 2, 400.2 Hz

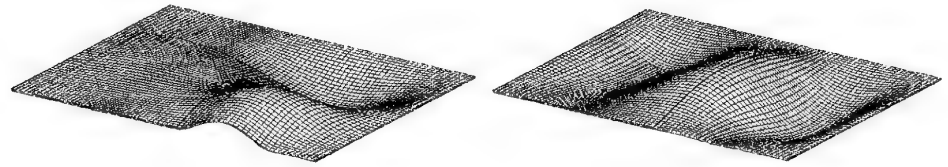

Mode 3, 554.4 Hz

Mode 4, 674.3 Hz

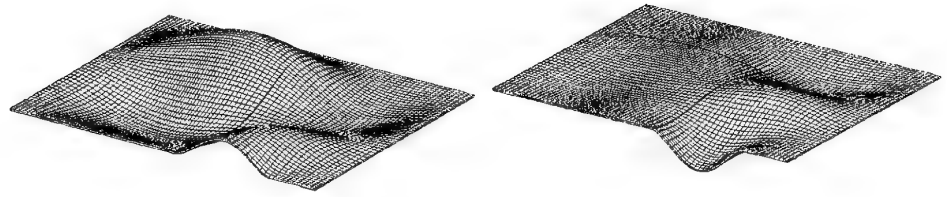

Mode 5, 757.1 Hz

Mode 6, 883.3 Hz

*Figure 17. Mode shapes for the repaired panel containing a long crack (2a = 196mm).*

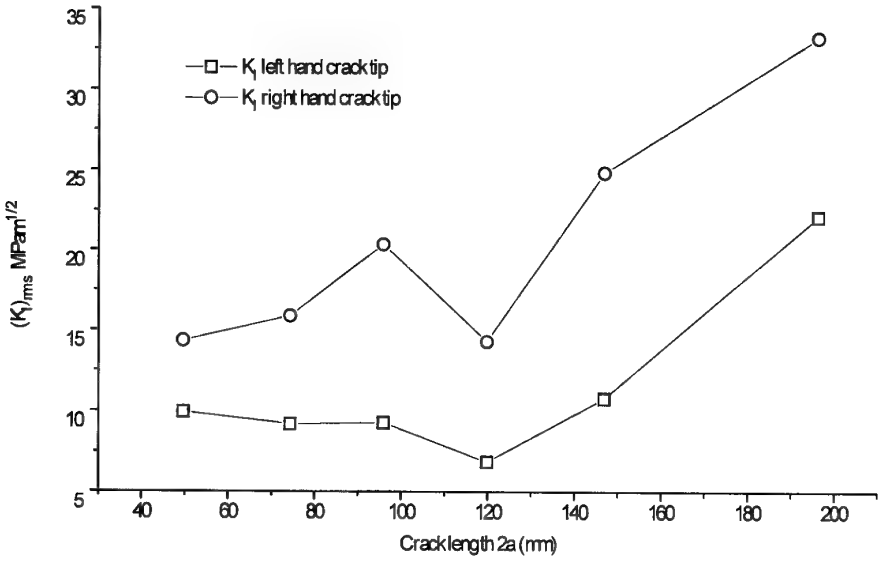


*Figure 18 (a) Stress intensity factor $(K_I)_{rms}$ in un-repaired panel for left and right hand crack tips*

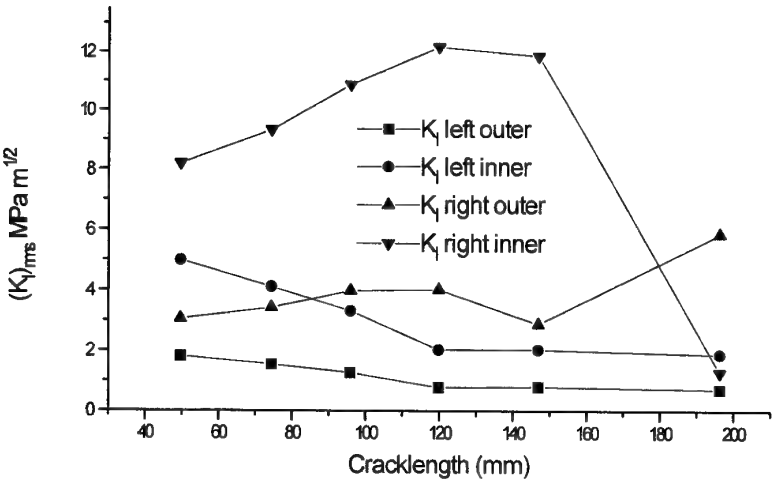


*Figure 18 (b) Stress intensity factor $(K_I)_{rms}$ in repaired panel. (Note the change in scale.)* The rms mode *II* stress intensity factor, $(K_{II})_{rms}$ for the cracked un-repaired panel is shown in Fig. 19a. Little through thickness variation of $(K_{II})_{rms}$ has been found, hence values are only

presented for each crack tip. Numerical values are similar to $(K_{II})_{rms}$ and the existence of $(K_{II})_{rms}$ explains the tendency of long cracks to turn into the centre of the panel. For the case of the repaired panel shown in Fig. 19b, $(K_{II})_{rms}$ has been substantially reduced.

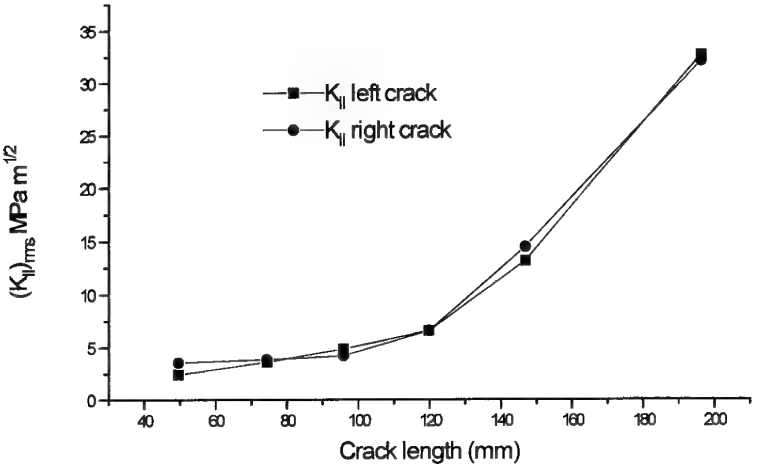


*Figure 19 (a) Stress intensity factor $(K_{II})_{rms}$ for un-repaired panel.*

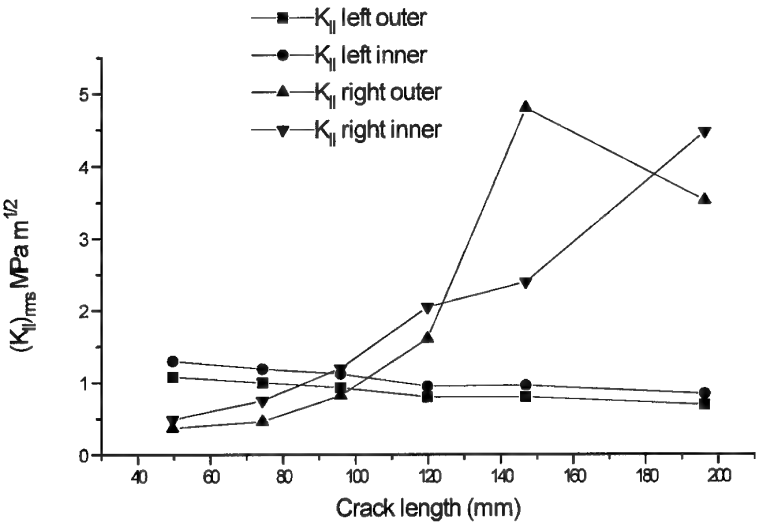


*Figure 19 (b) Stress intensity factor $(K_{II})_{rms}$ for repaired panel.(note the change in scale).*

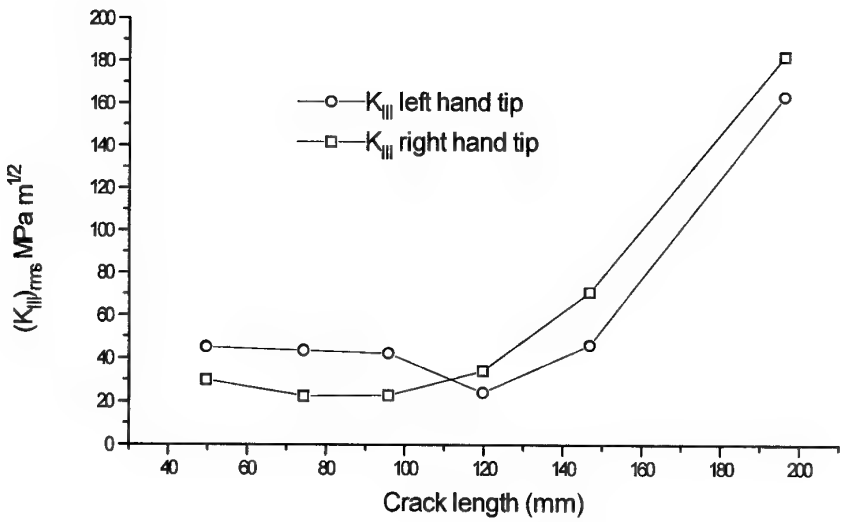


*Figure 20 (a) Stress intensity factor $(K_{III})_{rms}$ for un-repaired panel.*

The rms of mode *III* stress intensity factor $(K_{III})_{rms}$ for the cracked un-repaired panel is shown in Fig. 20a. The values of $(K_{III})_{rms}$ increase significantly with crack length for both left and right hand crack tips, and the numerical value of $(K_{III})_{rms}$ is greater than $(K_I)_{rms}$. Clearly $(K_{III})_{rms}$ will contribute significantly to crack growth. In the case of the repaired panel, shown in Fig. 20b, the values of $(K_{III})_{rms}$ for a crack tip under the patch are low, but not zero. However, once the crack grows outside the patch (i.e. for crack lengths > 120 mm) $(K_{III})_{rms}$ increases significantly.

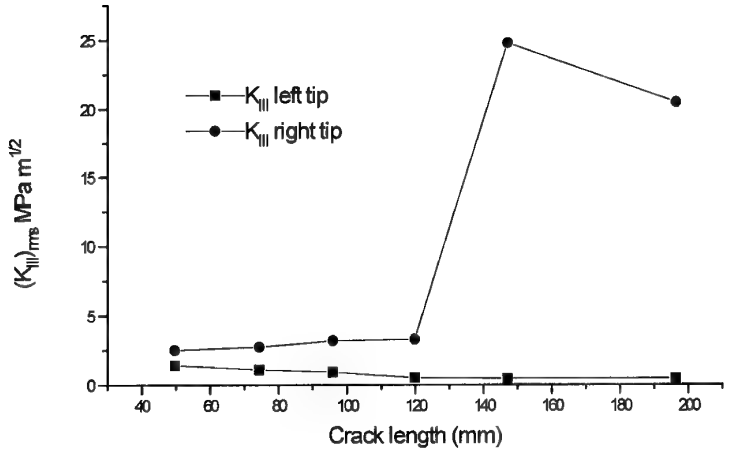


*Figure 20 (b) Stress intensity factor $(K_{III})_{rms}$ for repaired panel.(note the change in scale).*

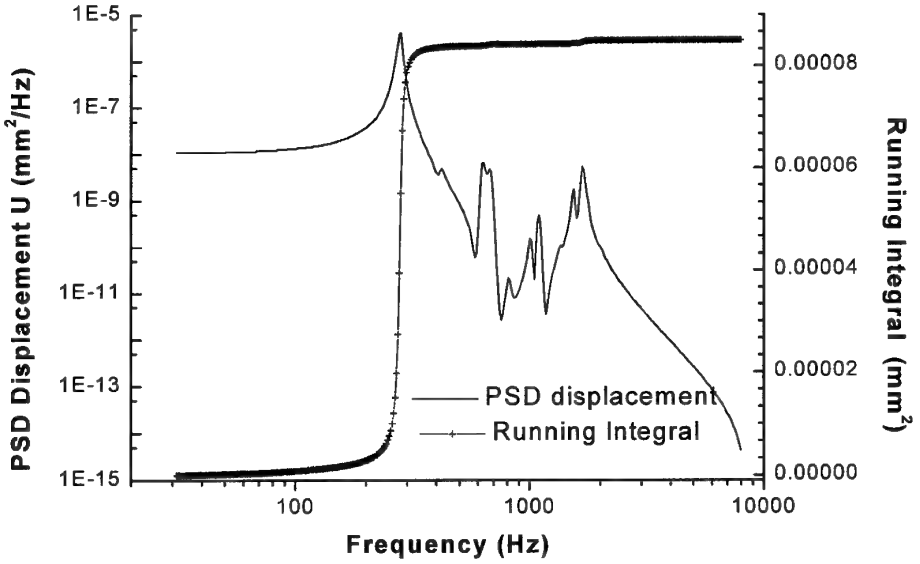


*Figure 21(a) PSD of displacement ( $\alpha\ (K_I)_{rms}$ ) and running integral of the PSD for repaired panel of crack length 2a=50 mm.*

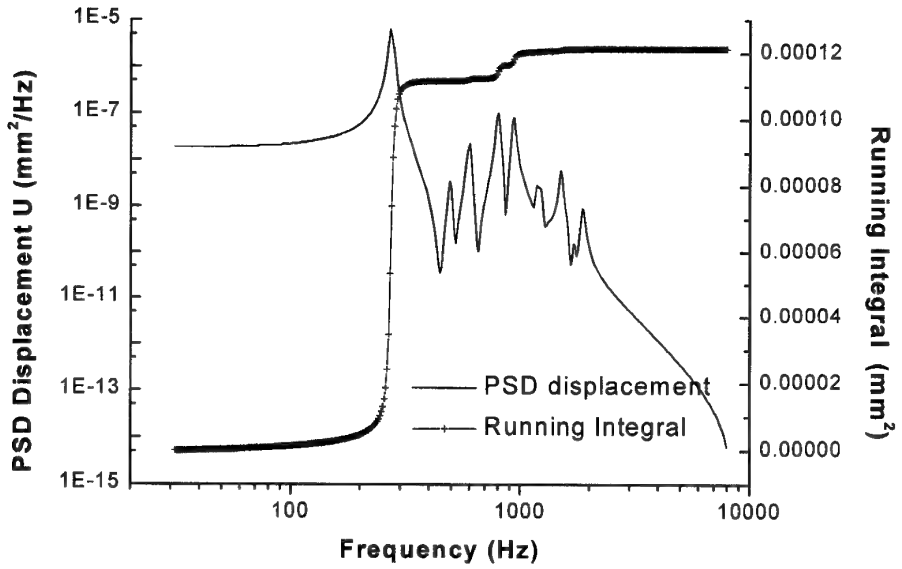


*Figure 21(b) PSD of displacement ($\alpha\ (K_I)_{rms}$) and running integral of the PSD for repaired panel of crack length 2a=196 mm.*

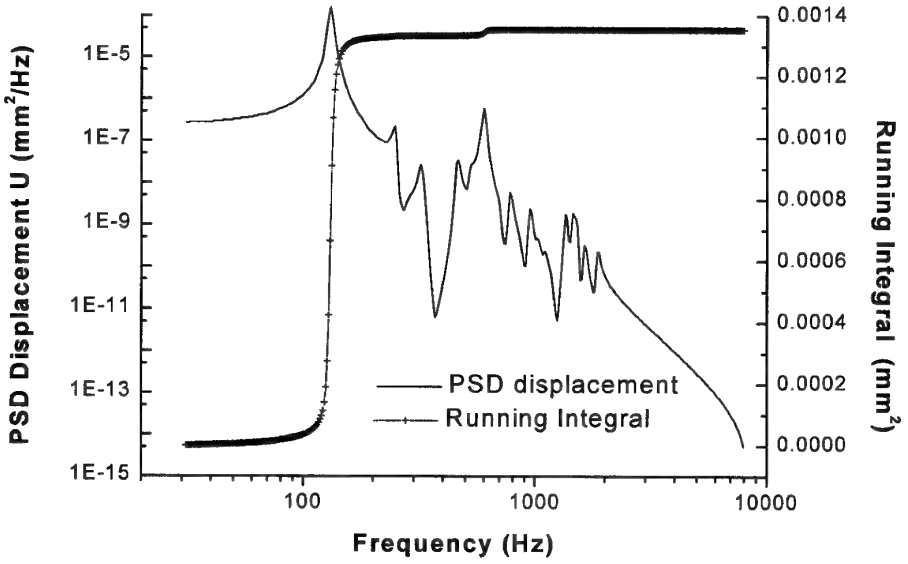


*Figure 21(c) PSD of displacement ($\alpha\ (K_I)_{rms}$) and running integral of the PSD for un-repaired panel with crack length 2a=196 mm.*

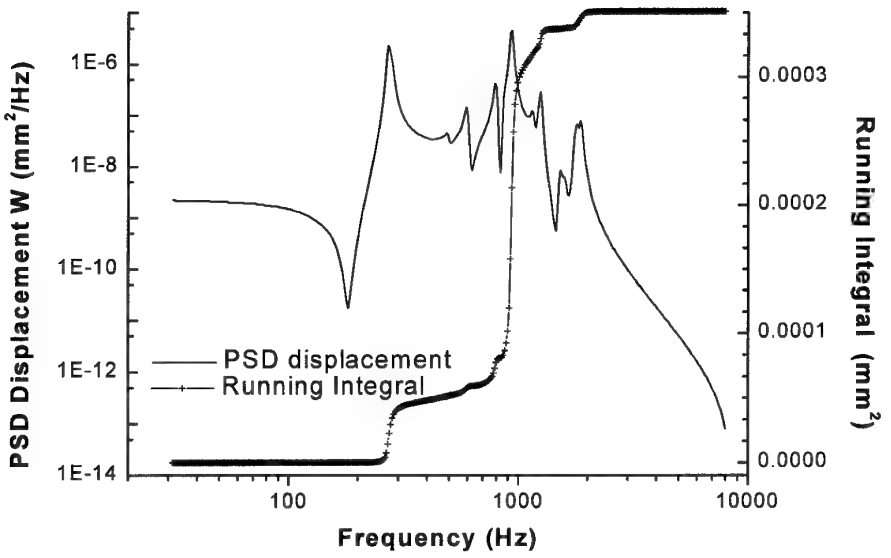


*Figure 21(d) PSD of displacement ($\alpha\ (K_{III})_{rms}$) and running integral of the PSD for repaired panel of crack length 2a=196 mm.*

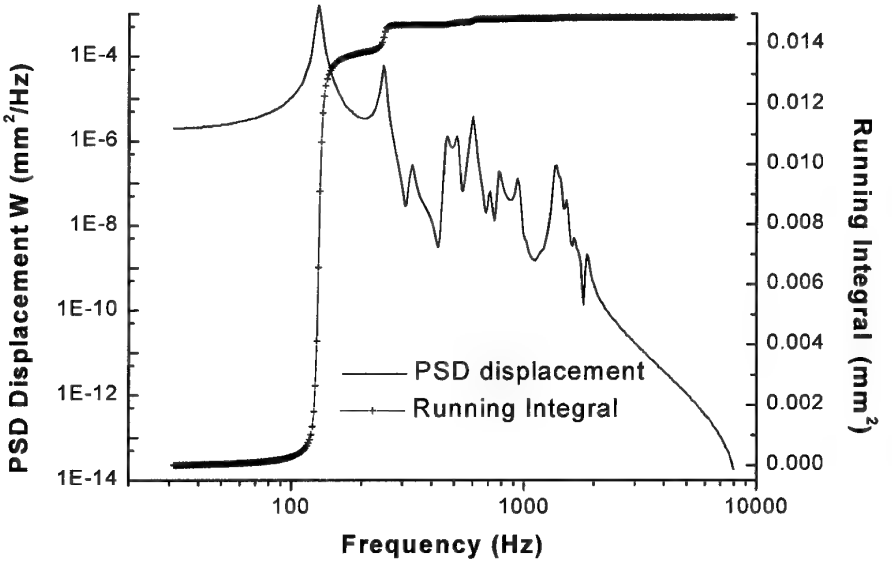


*Figure 21(e) PSD of displacement ($\alpha\ (K_{III})_{rms}$) and running integral of the PSD for un-repaired panel of crack length 2a=196 mm.*

Fig. 21 shows PSD of the displacement response u and w behind the right hand crack tip for various cracked repaired/un-repaired scenarios. Equs 3-5 imply that the u and w response are proportional to the $(K_I)_{rms}$ and $(K_{III})_{rms}$ responses respectively. Therefore the PSD shown in Fig. 21 indicate the relative response of $K$ with increasing frequency. Fig. 21 (a)-(c) shows the $(K_I)_{rms}$ frequency response for repaired and un-repaired panels containing cracks of various lengths. Fig. 21 (d) & (e) show the $(K_{III})_{rms}$ frequency response for repaired and un-repaired panels for a crack length of 196mm, respectively.

Fig. 21(a) shows the PSD for the case of a repaired panel with $2a=50$ *mm*. In this case each peak will correspond to the resonant frequencies illustrated in Fig. 16. For example the fundamental resonant mode occurs at a frequency of 280 Hz in Fig. 16 which corresponds to the maximum response in Fig. 21(a). Absence peaks at certain resonances, eg Mode 2 at 414.5 *Hz*, indicates that the crack tip is located at or near the nodal line of the corresponding mode shape. A running integral of the PSD response will indicate the relative contribution of each of the modes to the overall $K_{rms}$ and is also shown in Fig. 21. Fig. 21(a) shows that 98% of the overall $(K_I)_{rms}$ is due to the first mode corresponding to the repaired panel of cracklength 2a = 50mm.

In the case of the repaired panel containing a long crack of 196 *mm* the response for $(K_I)_{rms}$ is shown in Fig. 21(b). It is evident from the running integral that mode 1 makes the major contribution to the overall $(K_I)_{rms}$ response followed by modes 4 and 5. However the response for $(K_{III})_{rms}$ shown in Fig. 21(d), clearly shows that mode 6 makes the major contribution to the overall $(K_{III})_{rms}$ response at a frequency of 883 *Hz*, followed by mode 1. In the case of long cracks in the un-repaired panel, the response for $(K_I)_{rms}$ and $(K_{III})_{rms}$ is shown in Figs. 21(c) and 21(e), respectively. In these cases once again mode 1 makes the major contribution to these parameters.

## 4.3 Summary of Repair Failure Investigation

The fractographic anaylsis indicates that before the panel was repaired the mode III stress intensity provided the crack tip driving force. However after the repair, transverse bending of the panel resulted in a mode I stress intensity factor at the skin surface providing 98% of the crack tip driving force. Interestingly, the crack growth after the repair was significantly higher than before the repair. It is possible that the rubbing of the crack faces provided friction damping to the system, which did not occur under mode I. The analysis carried out has simulated and characterised the growth of the crack in both the cracked unrepaired and cracked repaired panel. It was found that a relatively high stress intensity factor still existed on the inner surface of the right hand crack tip after the repair was applied. This value was $12MPa\sqrt{m}$ compared to a value of $35MPa\sqrt{m}$ for the unrepaired panel. For an aircraft component subjected to manoeuvre and gust loads this reduction in stress intensity factor would have been adequate, however crack growth corresponding to a fundamental frequency of 300Hz will be significant.

# 5. Highly Damped Repairs for Cracked Panels

The work carried out in this section is based on [5]. It is evident from the previous section that a change in direction is necessary to design an effective long term solution for bonded composite repair systems subject to acoustic loading conditions.

## 5.1 Design of Highly Damped Patch

The cracking surveys undertaken by Rodgers et al [3] indicates that typical crack lengths, before repair, are 100 mm long and occur in a skin thickness of approximately 1 mm. The repair must restore the stiffness of the structure, with an equivalent amount of composite material, and also reduce the dynamic stress levels using high damping (VEM).

Since the repairs are on the external surface there is a requirement to preserve aerodynamic smoothness. Therefore patch development is undertaken with the restriction that the patch must be tapered and the thickness must not exceed approximately 3 mm (1/8"). Rogers et al [6] considered this to be an adequate thickness since such an intrusion would not be significant with respect to the boundary layer thickness expected at that location. In addition the possible crack growth for a 6000 hour lifetime must be considered.

The process of designing a highly-damped patch is illustrated by the flow chart shown in Fig 22. The analysis begins with the definition of geometry, boundary conditions and appropriate material loss factors for the F.E. model of the cracked structure. The model is also subject to the input pressure PSD. Also incorporated within the model is the repair configuration to restore structural integrity. After the F.E. analysis is carried out, the rms stresses, strains, displacements and stress intensities must be considered. From crack growth data the likely crack size after 6000 hours in-service can be estimated. If the crack growth exceeds the limit required at 6000 hours then a new (damping) material and geometric configurations must be considered. Clearly the damping material must be capable of achieving the assumed loss factor under the expected operating temperatures. That is, a reasonable estimate of the operating temperature is required since the material loss factor of the VEM is highly dependent on the operating temperature. Therefore accurate crack growth predictions will depend on accurate measurements of (i) load and strain levels, and resonant frequencies (needed to calibrate the F.E. model), (ii) operating temperature and VEM data and (iii) crack growth data (generated under high frequency bending conditions). The flow chart illustrates the systematic procedure used for changing the configuration until an acceptable design is achieved.

## 5.2 Damping of Highly Damped Patch

One of the most effective mechanisms to substantially reduce the dynamic stress level in the repaired structure is to increase the damping performance of the repair and, therefore, of the repaired structure. Callinan et al [4,5], Rogers et al [6] and Liguour et al [7] reported on the use of a highly-damped composite patch (or 'Durability Patch') to prevent the further growth of costly 'nuisance' cracks. This is a passive damping technique aimed at reducing

high-cycle fatigue. Rogers et al [6] noted that this type of application was rarely used for high-cycle fatigue because the necessary design information such as temperatures, resonant frequencies, and strain levels were difficult to obtain. They further reported that aircraft structures are often susceptible to resonant high-cycle fatigue due to the low intrinsic damping of the material since rms stress levels are highly dependant on modal damping. Thus in order to increase damping the authors considered the use of constrained layer damping which increases the structural damping of the repaired structure and will assist in stopping or substantially reducing acoustically-induced crack growth in the panel.

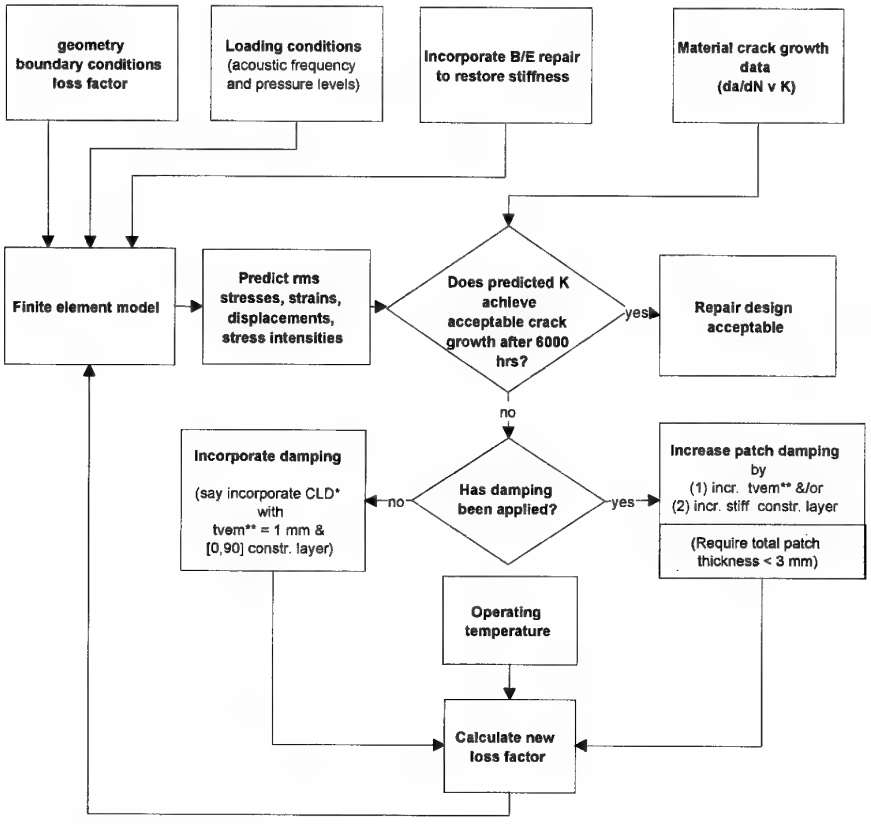


* CLD - Constrained layered damping
** tvem - viscoelastic material thickness (select VEM with highest loss factor at required operating temperature)

*Figure 22. Flow chart for designing highly-damped repairs for acoustically-induced cracked skins.*

There are numerous case studies, noted by Soovere & Drake [12], of the use of damping in the aeronautical scene to alleviate problems associated with resonant vibrations. In this section the modal loss factor of a reinforced panel is calculated for various bonded doubler reinforcement geometries, add-on damping treatment geometries and constraining layer effective stiffnesses. This damping study is undertaken on a panel similar to that shown in Fig. 14 except that no crack is present and the reinforcement now has its centreline (i.e. the centre of the W dimension) aligned with the centreline of the long dimension of the panel.

Initially an investigation into the effect of reinforcement geometry on modal loss factor is undertaken. In this case a 250 mm long by 166 mm wide by 1.2 mm thick aluminium panel, fixed on all four sides, is modelled. The entire aluminium panel is treated with a layer of constrained layer damping. Typical 'off-the-shelf' constrained layer damping treatments are 0.5 to 2 mm thick with a 0.125 mm thick constraining layer of aluminium. Material properties for the damping (VEM) material, aluminium alloy and boron/epoxy are given in Table 2. The material loss factor for the viscoelastic material is taken as 1.0 and the constraining layer is an aluminium sheet 0.125 mm thick. The panel is reinforced with a unidirectional boron/epoxy laminate with fibres aligned in the y-direction, see Fig. 14. The thickness of this reinforcement is determined such that the stiffness of the reinforcement and the aluminium plate are matched, i.e. using equation (8):

$$E_{al}t_{al} = E_r t_r \tag{8}$$

These studies were conducted with a reinforcement of constant length (L) of 75 mm and varying widths (W) of 50 mm, 100 mm and 125 mm. The effects of these different size reinforcements on the structural loss factor of the panel are determined and are given in Table 3. It must be pointed out at this stage that the damping properties of the boron/epoxy laminate are not included in the analysis. Therefore, the actual structural damping is expected to be higher than that predicted in this study, hence, the results from this study are conservative. The modal loss factor is calculated from the finite element analysis by assuming that, given the material damping, the modal structural loss factor [17] can be calculated by:

$$\eta_S = \sum_{i=1,n} \eta_i e_i / e \tag{9}$$

where $\eta_S$ is the structural loss factor and $\eta_i$ is the material loss factor of the $i$ th element. The modal energy, $e$, is calculated with equation (10):

$$e = \int \delta^T [K] \delta dV \tag{10}$$

Where $\delta$ is the eigenvector and the stiffness matrix is denoted by [K]. Equation (9) is implemented as a post-processing option in our finite element analysis package and was first validated prior to its use.

The results in Table 3 show that the size of the unidirectional boron/epoxy reinforcement has a small effect on the structural damping. However, [13] observed that when the reinforcement was made from aluminium changing the size of the reinforcement caused a large change in the modal loss factor. For example, when the size of the boron/epoxy reinforcement is increased from 75 mm by 50 mm to 75 mm by 125 mm, there is only a 5 % reduction in the modal loss factor for mode 1 compared to an 11 % reduction for the aluminium reinforcement.

Table 4 shows the results for modal loss factors when only the boron/epoxy patch is treated with constrained layer damping. This table shows that the structural damping derived with this scheme of damping treatment is not very effective. These results therefore confirm that damping treatment should be applied to the entire panel for more effective damping of the structure.

The investigation is extended to a panel with dimensions shown in Fig. 14 without the crack and with the reinforcement centred as described above. In this analysis only one patch size is considered, viz. 77 mm long by 125 mm wide, but the VEM thickness, $t_{VEM}$, is varied from 0.5 mm to 2.0 mm. The constraining layer is now boron/epoxy and two laminates are modelled, viz. a 2 ply [0/90] laminate and a 4 ply $[0/90]_{sym}$ laminate.

*Table 3 - Loss factor of aluminium panel (with no crack) reinforced with unidirectional boron/epoxy with a 1 mm thick damping treatment and 0.125 mm thick aluminium constraining layer applied to whole panel.*

| Mode | Damped natural frequency (Hz) | Loss factor | Specimen description |
|---|---|---|---|
| 1 | 290 | 0.139 | Patch dimensions are |
| 2 | 460 | 0.113 | 75 mm (L) x 50 mm (W) |
| 3 | 769 | 0.081 | |
| 1 | 288 | 0.135 | Patch dimensions are |
| 2 | 441 | 0.118 | 75 mm (L) x 100 mm (W) |
| 3 | 723 | 0.093 | |
| 1 | 289 | 0.132 | Patch dimensions are |
| 2 | 442 | 0.116 | 75 mm (L) x 125 mm (W) |
| 3 | 732 | 0.085 | |

The predicted results are given in Table 5. Table 5 shows a significant increase in modal loss factor as the VEM thickness is increased. For mode 1 an increase of 32 % and 90 % is observed when the VEM thickness is increased from 0.5 mm to 1.0 mm and 0.5 mm to 2 mm, respectively. With the increase in thickness of the VEM there is also a corresponding drop in damped natural frequency which is mainly due to the increase in mass. Also increasing the effective stiffness of the constraining layer substantially improved the modal loss factor of the panel. For the 1.0 mm thick VEM case the loss factor, for the first resonant mode, increased by 34 % when the effective stiffness of constraining layer is increased by substituting the [0/90] laminate with a $[0/90]_{sym}$ laminate. The increase in loss factor is less pronounced for the 2.0 mm thick VEM case where an increase in 18% was observed when the constraining layer thickness is increased from 2 to 4 plies.

*Table 4 - Loss factor of aluminium panel (with no crack) reinforced with unidirectional boron/epoxy with a 1 mm thick damping treatment and 0.125 mm thick aluminium constraining layer applied to the reinforcement only.*

| Mode | Damped natural frequency (Hz) | Loss factor | Specimen description |
|---|---|---|---|
| 1 | 324 | 0.03 | Patch dimensions are |
| 2 | 543 | 0.011 | 75 mm (L) x 50 mm (W) |
| 3 | 852 | 0.022 | |
| 1 | 316 | 0.049 | Patch dimensions are |
| 2 | 501 | 0.03 | 75 mm (L) x 100 mm (W) |
| 3 | 833 | 0.036 | |
| 1 | 315 | 0.053 | Patch dimensions are |
| 2 | 492 | 0.036 | 75 mm (L) x 125 mm (W) |
| 3 | 830 | 0.036 | |

*Table 5 - Loss factor of aluminium panel (with no crack) reinforced with a unidirectional boron/epoxy patch of dimensions 77 mm (L) x 125 mm (W) with the constrained layer damping treatment applied to whole panel.*

| Mode | Damped natural frequency (Hz) | Loss factor | Specimen description |
|---|---|---|---|
| 1 | 258 | 0.122 | |
| 2 | 449 | 0.106 | $t_{vem}$ = 0.5mm |
| 3 | 641 | 0.078 | [0/90] boron/epoxy constraining layer |
| 1 | 240 | 0.161 | |
| 2 | 411 | 0.132 | $t_{vem}$ = 1.0 mm |
| 3 | 597 | 0.091 | [0/90] boron/epoxy constraining layer |
| 1 | 217 | 0.232 | |
| 2 | 368 | 0.178 | $t_{vem}$ = 2.0 mm |
| 3 | 528 | 0.126 | [0/90] boron/epoxy constraining layer |
| 1 | 245 | 0.216 | |
| 2 | 423 | 0.163 | $t_{vem}$ = 1.0 mm |
| 3 | 585 | 0.122 | $[0/90_{sym}]$ boron/epoxy constraining layer |
| 1 | 222 | 0.274 | |
| 2 | 378 | 0.203 | $t_{vem}$ = 2.0 mm |
| 3 | 528 | 0.100 | $[0/90_{sym}]$ boron/epoxy constraining layer |

Overall this theoretical study has shown that the modal loss factor of the reinforced panel can be significantly improved by incorporating constrained layered damping. Further improvements can be achieved by increasing (i) the thickness of the VEM and (ii) the effective stiffness of the constraining layer. The values of modal loss factor of panels incorporating highly-damped patches, tabulated in Table 5, are used in the next section as inputs for the FE models of repaired cracked panels.

## 5.3 Results for Unrepaired Cracked Plate

Previously we have established that in section 3 the stress intensity in the cracked (unrepaired) plate is as shown in Fig. 18. Specifically the most relevant data is that given in Fig. 18a. Here the right hand crack tip refers to the crack tip located midway along the plate

shown in Fig. 14. The higher stress intensity for the right hand crack tip is due to the larger dynamic bending stresses that occur midway along the panel. For a crack length of 80 mm, $K_I$ =15 MPa$\sqrt{m}$. Although this is not a high value in comparison with the fracture toughness value, $K_{IC}$, in an environment of high-cycle fatigue it leads to a high crack growth rate.

## 5.4 Analysis of Highly Damped Repair to a Cracked Plate

The F.E. analysis is carried out as previously done in section 4.1. The behaviour of the plate, adhesive and viscoelastic damping materials are modelled as a 3 dimensional element, to allow for shear deformation. The boron/epoxy patch and boron/epoxy constraining layer are sufficiently thin such that 2D shell elements are an adequate representation.

The geometry of the structure is shown in Fig. 14. The mesh size of the skin and viscoelastic structure is 75x60 elements. As shown, the unidirectional boron/epoxy reinforcing patch only extends partially across the panel. It also covers an adjacent panel as shown in the dotted outline. The boron/epoxy repair has length, L, and width, W. In this section the length is fixed at 77 mm, however three widths are considered, viz. 80 mm, 99 mm and 126 mm. The entire panel is covered with the CLD material. Material properties for the skin, adhesive, damping material and boron are shown in Table 3.

The boundary conditions for this model are considered to be fully clamped except for the crack region which is not restrained. The patch above the crack also remains fully constrained. Clearly crack closure will occur at an increasing distance away from the crack tip, however the complexity in introducing such constraints is not included in this preliminary study.

## 5.5 Results and Discussion

*Table 6 - Frequencies for original uncracked unrepaired plate.*

| Mode | Resonant frequency (Hz) |
|---|---|
| 1 | 218 |
| 2 | 374 |
| 3 | 506 |
| | |

*Table 7 - Resonant frequencies for various patch widths (W) and thicknesses of damping material with [0/90] boron/epoxy constraining layer. (* a/b refers to values of $t_{VEM}$/W in mm.)*

| | Case 1.0/80* | Case 1.0/126* | Case 2.0/80* | Case 2.0/126* |
|---|---|---|---|---|
| Mode | Resonant frequency (Hz) | | | |
| 1 | 208 | 216 | 193 | 200 |
| 2 | 335 | 341 | 308 | 319 |
| 3 | 442 | 461 | 403 | 417 |

### 5.5.1 Modal shapes and frequencies

One of the main concerns regarding a particular repair is the change of frequency of the plate since a stiffer structure may change the load path. The first three frequencies of the original uncracked unrepaired plate are shown in Table 6. For a highly-damped patch consisting of a 1.0 mm thick damping layer with a [0/90] boron/epoxy constraining layer the variation of resonant frequencies with increasing patch width (W) is shown in Table 7. The reinforcing patch length (L) is 77 mm. In all cases the addition of the highly-damped patch configuration resulted in a reduction of frequency. The resonant frequency increases by 5 %, 10 % and 13 % for vibration modes 1, 2 and 3, respectively, when the patch width increased from 80 to 126 mm. The first three modes are shown in Figs. 23, 24 and 25. The resonant frequencies for a 2.0 mm thick damping layer with a [0/90] boron/epoxy constraining layer for various patch widths (W) are shown in Table 7

.

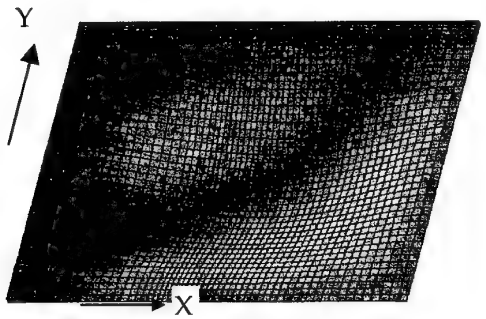


*Figure 23. Mode shape for mode 1 (211 Hz).*

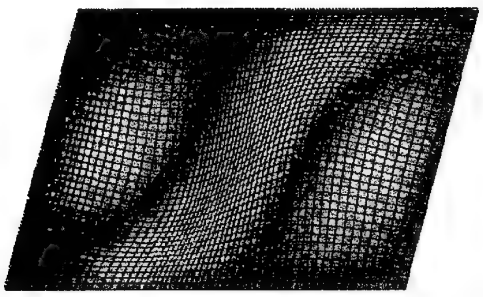

*Figure 24. Mode shape for mode 2 (335 Hz).*

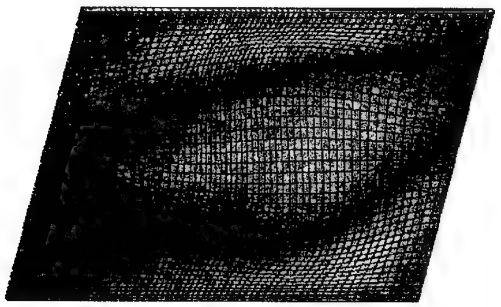

*Figure 25. Mode shape for mode3 (458 Hz).*

### 5.5.2 PSD of the displacement

Since the area under the displacement PSD curve is the mean square displacement response, then a running integral of the displacement PSD illustrates the contribution of each vibration mode to the overall displacement response, as shown in Fig. 26. Since the stress intensity is proportional to the crack opening displacement, then a running integral of the displacement response will indicate the contribution of each vibration mode to the overall stress intensity. Fig. 26 shows the PSD displacement response at the right hand (inner side) crack for the case of a 1.0 mm thick damping layer with [0/90] boron/epoxy constraining layer and a 80 mm wide by 77 mm long boron/epoxy patch. Fig. 26 shows that vibration mode 1 contributes up to 99% of the overall stress intensity.

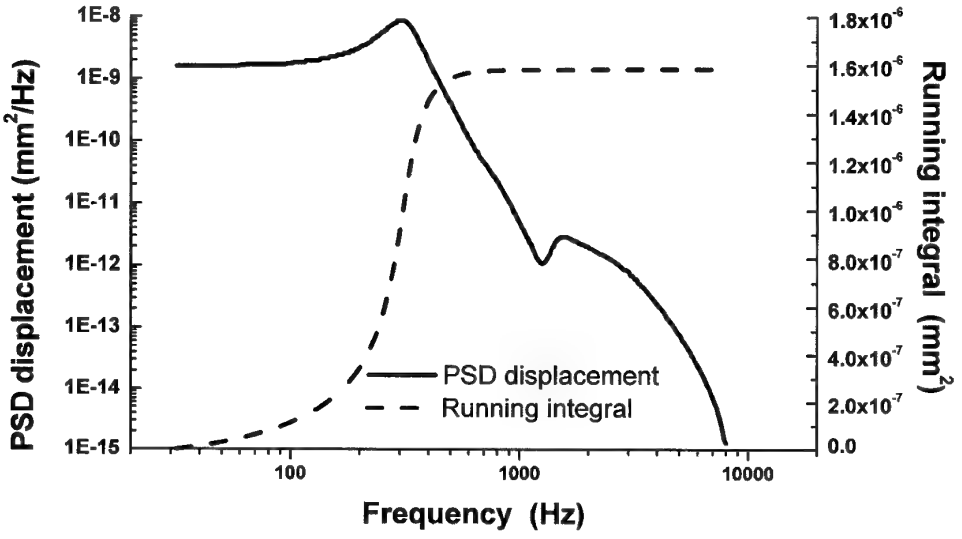


*Figure 26. PSD of displacement ( $\alpha\ (K_I)_{rms}$ ) and running integral of the PSD for a panel with a 1.0 mm thick damping layer with [0/90] boron/epoxy constraining layer and a 80 mm wide by 77 mm long boron/epoxy reinforcement.*

### 5.5.3 Stress intensity factor

Stress intensity factors are computed at the inside and outer surfaces of the skin. Since the repair results in a neutral axis shift the maximum values exist at the inner surface. The most critical crack tip position is the tip located midway down the longest side of the panel, as shown in Fig. 14. The maximum values have been plotted in Figs. 27, 28, 29 and 30. Various highly-damped patch configurations, involving 0.5, 1.0 and 2.0 mm thick damping VEM, are considered. In all cases the highly-damped patch has a boron/epoxy reinforcement/repair with dimensions 77 mm long and varying widths of 80 mm, 99 mm and 126 mm. Over the range of damping thickness considered the configuration that give the lowest values of $(K_I)_{rms}$ is for the 77 mm long by 126 mm wide reinforcement/repair with the 1.0 mm thick VEM and [0/90] constraining layer case. Also, the 0.5 mm thick VEM with [0/90] constraining layer case gave similar stress intensities as shown in Fig. 28.

Although no crack growth data corresponding to $(K_{II})_{rms}$ or $(K_{III})_{rms}$ stress intensities are available, the numerical values of $(K_{II})_{rms}$ are lower than those for $(K_I)_{rms}$, as shown in Fig. 29. Also, the numerical values for $(K_{III})_{rms}$, as shown in Fig. 30, are numerically comparable to $(K_I)_{rms}$. All of the damped repairs are equally effective in reducing $(K_{II})_{rms}$, and show a considerable reduction in comparison to the low damped design. Also the results for $(K_{III})_{rms}$ show that all the configurations, except the 0.5 mm, [0/90] configuration, gave equally low values of $(K_{III})_{rms}$. Overall, comparisons with the low damped patch, i.e. a repair with no CLD included, have shown the highly-damped patch to be very effective. The best overall results appear to be for the 1.0 mm [0,90] configuration.

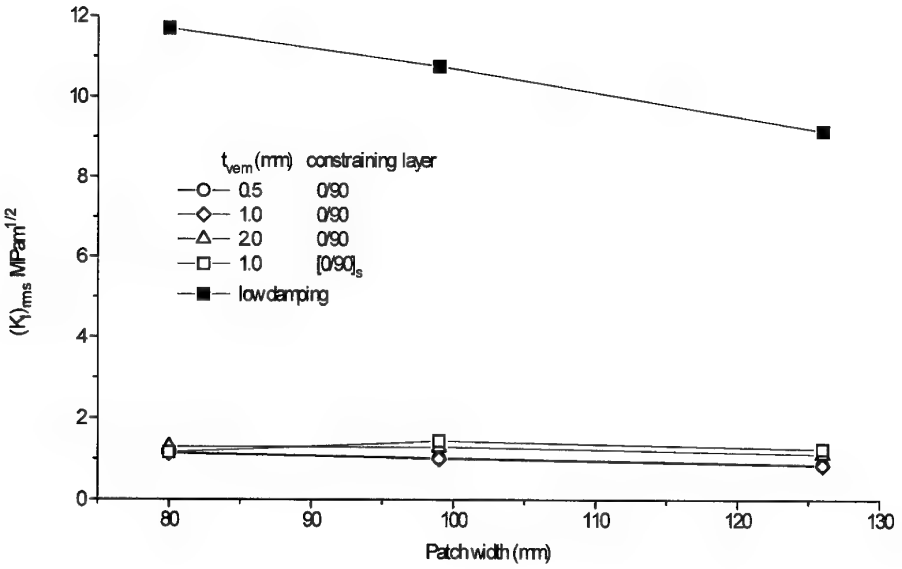


*Figure 27. Stress intensity factor, $(K_I)_{rms}$, for various highly-damped and low damped patch configurations.*

### 5.5.4 Crack growth predictions

The crack growth data shown in Fig. 31 is for 7075-T6 corresponding to long crack growth data for panels tested in uniaxial tension [14]. As a result of the neutral axis offset the curve of $R = 0$ most closely represents the crack growth curve. While these data are for low frequency loading conditions, evidence exists that high frequency testing results in slightly lower crack growth rates, [15,16]. In our case high frequency bending is involved, therefore taking crack growth rates from Fig. 31 will lead to conservative estimates of crack length. The curve in Fig. 31 has been extrapolated to determine the approximate crack growth rate for cases less than $10^{-8}$ mm/cycle. Using these data insignificant crack growth has been calculated, after the 6000 hrs, for all the highly-damped patch configurations considered. Crack growth data for 4% Cu-Al alloy subjected to high frequency bending, given in reference [16], also indicates negligible crack growth for all the highly-damped patch configurations considered. Although no crack growth data corresponding to $K_{II}$ or $K_{III}$ stress intensities are available the $K_{III}$ results shown in Fig. 30 indicate possible crack growth for the 0.5 mm [0,90] configuration. Note that the above results are highly dependent on the material loss factors used in the modelling. This loss factor is also dependent on the operating temperature. Therefore in order to design an effective highly damped repair knowlegde of the temperature condition when the high SPL are generated is required.

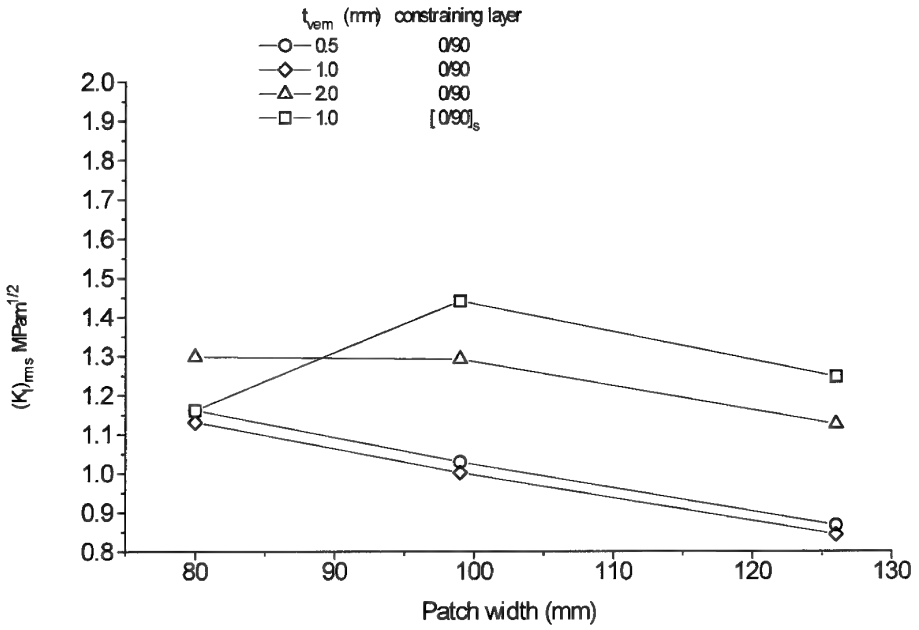


*Figure 28. Stress intensity factor, $(K_I)_{rms}$, for various highly-damped patch configurations.*

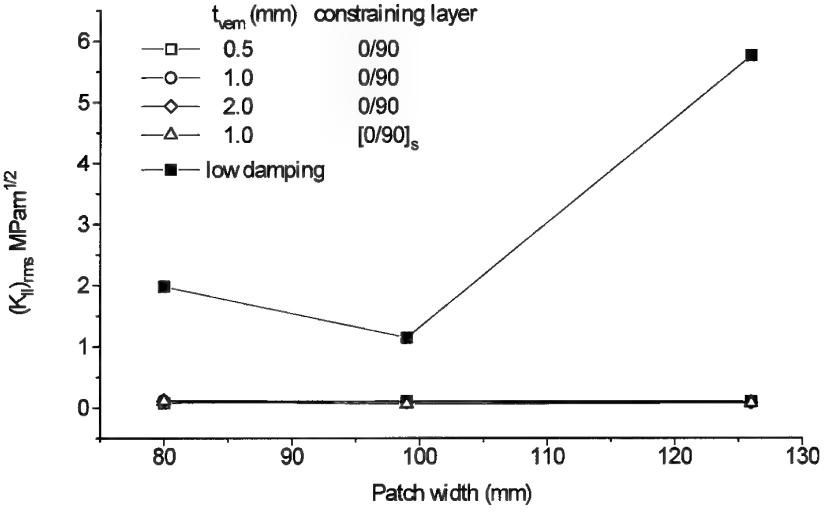


*Figure 29. Stress intensity factor, $(K_{II})_{rms}$, for various highly-damped and low damped patch configurations.*

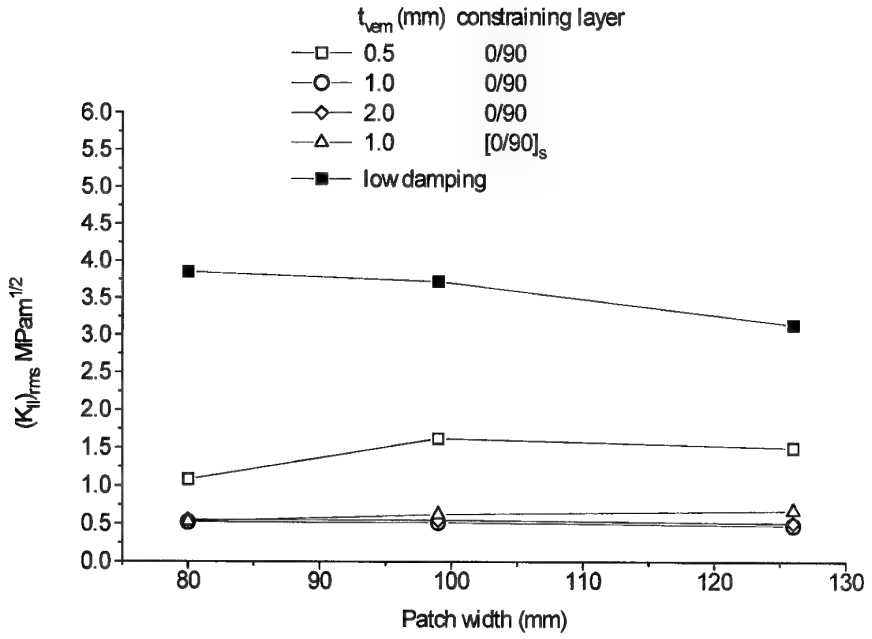


*Figure 30. Stress intensity factor, $(K_{III})_{rms}$, for various highly-damped and low damped patch configurations.*

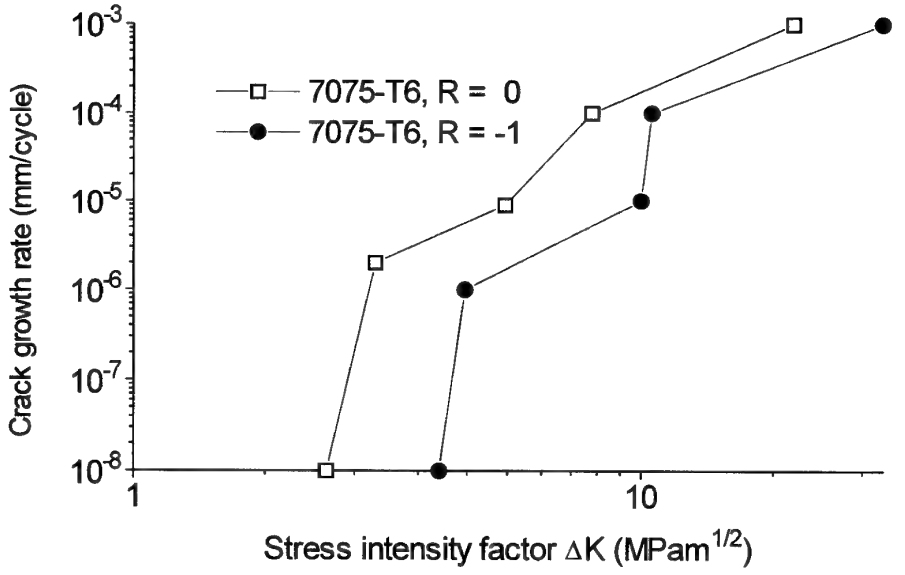


*Figure 31. Crack growth rate for 7075-T6 with increasing $K_I$, ref [14].*

# 6. Conclusions

An investigation into the failure of a boron/epoxy repair of an aluminium panel subject to acoustic fatigue has revealed that after the repair sufficiently high stress intensities existed to promote crack growth. A fractographic analysis has revealed that the cracks in the panel initiated at a single site on the inside surface of the thicker section. Furthermore the application of a boron/epoxy repair changed the crack growth mode from mode III to mode I. The rubbing of the crack faces under mode III would be expected to result in some damping, and this may explain the lower crack growth rate before the repair.

A methodology is proposed to enable the design of highly-damped patches for cracked structures subject to intense acoustic loading. The highly-damped patch incorporates a boron/epoxy reinforcement/repair, to restore structural strength, as well as a constrained damping layer in order to enhance damping and thus reduce dynamic stresses. The proposed highly-damped patches reduce the response at resonance of the patched panel compared to the unrepaired cracked panel. A study investigating the effects of various reinforcement dimensions, VEM thicknesses and constraining layer configurations on the modal loss factor of the plate has also being undertaken. It was found that for the various reinforcements studied, no significant variation in loss factor was observed. However significant increases in loss factor are observed with increasing VEM thickness and constraining layer effective stiffness. The inclusion of damping in the repair enables the stress intensity factor to be substantially reduced. Predictions of $K_I$ indicates that no crack growth is expected for all the highly-damped patched configurations considered.

# 7. Acknowledgments

The authors would like to acknowledge Mr. Steve Sanderson of AED for assistance in the finite element analysis.

# 8. References


(1) A/B/C/D Aircraft Lower Nacelle Skin Acoustic and Strain Measurements and Sonic Fatigue Analysis. MDC 94B0044. MACAIR, U.S.A. Mar, 1994.

(2) A. A Baker, "Bonded Composite Repair of Metallic Aircraft Components", AGARD-CP-550 Composite Repair of Military Aircraft Structures, Paper 1, 1994.

(3) Composite Materials and Adhesive Bonded Repairs. RAAF Standard Engineering C5033, January 1994.

(4) R.J. Callinan, S.C. Galea and S. Sanderson. Finite element analysis of bonded repairs to edge cracks in panels subjected to acoustic excitation. Composite Structures vol. 38, no. 1-4, p. 649-600, 1997.

(5) R.J. Callinan, W.K. Chiu and S.C. Galea. Optimisation of a Composite Bonded Repair to Cracked Panels Subjected to Acoustic Excitation. Proceedings of the 21st Congress of the Aeronautical Sciences (ICAS 98) Melbourne, Australia, 1-18 September 1998. (Paper A98-31631 ICAS Paper 98-5,3,2)

(6) L. Rogers, J. Maly, I.R. Searle, R.I. Begami, W. Owen, D. Smith, R.W. Gordon, D. Conley. Durability patch: Repair and life extension of high-cycle fatigue damage on secondary structure of ageing aircraft, 1st Joint DoD/FAA/NASA Conference on Aging Aircraft, Ogden, Ut, 8-10 July 1997.

(7) S. Liguour, R. Perez, K. Walters. Damped composite bonded repairs for acoustic fatigue, AIAA Paper 97-1689(A97-26775) AIAA/CGAS Aeronautics Conference, 3rd, Altanta, GA, May 12-14 1997, pp 774-783.

(8) N. Goldsmith. Examination of Cracked Panel from an F/A-18 Fuselage. DSTO DDP-0316, Aug., 1988.

(9) K. Blakely MSC/NASTRAN, Basic Dynamics Analysis, User's guide. The MacNeal-Schwendler Corporation, Dec,1993.

(10) H. Climent and J. Casalengua. Application of a PSD Technique to Acoustic Fatigue Stress Calculations in Complex Structures. Symposium on ' Impact of Acoustic Loads on Aircraft Structures', Lillehammer, Norway, May 1994.

(11) K.P. Byrne, Strains Affecting the Growth Rate of Edge Cracks in Acoustically Excited Panels. ISVR Tech. Rep. 59, Nov, 1972.

(12) J. Soovere and M.L. Drake. Aerospace Structures Technology Damping Design Guide - Volume II: Design Guide, AFWAL-TR-84-3089, 1985.

(13) W.K. Chiu, S.C. Galea and R.J. Callinan. Damping of repaired structures subject to acoustic fatigue. To appear in Polymers and Polymer Composites.

(14) J.C. Newman and P.R. Edwards. Short-Crack Growth Behaviour in Various Aircraft Materials. AGARD-12-767.

(15) A. Hartman, F.A. Jacobs, A. Nederven and P. de Rijk. Frequency Effect on 1mm 7075-T6 Clad Sheet. NLR TR M 2182, May 1967.

(16) K.P. Byrne, Bending-Induced Crack Propagation in a 4% Cu-Al Alloy with Reference to Acoustically Propagated Fatigue Cracks. Journal of Sound and Vibration, Vol 42, No 3, p. 337 - 355, 1975.

(17) C.D. Johnson and D.A.Kienholz. Finite Element Prediction of Damping in Structures with Constrained Viscoelastic Layers. AIAA Journal, Vol 20, No. 9, Sept. 1982.

DISTRIBUTION LIST

An Analytically Validated Highly Damped Repair for Acoustically - Induced Cracking on the F/A-18 Nacelle Skin

S. C. Galea and R. J. Callinan

**AUSTRALIA**

**DEFENCE ORGANISATION**

**Task Sponsor**
DGTA
**S&T Program**
Chief Defence Scientist
FAS Science Policy
AS Science Corporate Management
Director General Science Policy Development
} shared copy
Counsellor Defence Science, London (Doc Data Sheet)
Counsellor Defence Science, Washington (Doc Data Sheet)
Scientific Adviser to MRDC Thailand (Doc Data Sheet )
Scientific Adviser Policy and Command
Navy Scientific Adviser (Doc Data Sheet and distribution list only)
Scientific Adviser - Army (Doc Data Sheet and distribution list only)
Air Force Scientific Adviser
Director Trials

**Aeronautical and Maritime Research Laboratory**
Director

Chief of .Aircraft and Engines.. Division
Research Leader L.R.F.Rose
Author(s): S.C.Galea
R.J.Callinan

**DSTO Library**
Library Fishermans Bend (Doc Data sheet only)
Library Maribyrnong (Doc Data sheet only)
Library Salisbury
Australian Archives
Library, MOD, Pyrmont (Doc Data sheet only)
US Defense Technical Information Center, 2 copies
UK Defence Research Information Centre, 2 copies
Canada Defence Scientific Information Service, 1 copy
NZ Defence Information Centre, 1 copy
National Library of Australia, 1 copy

**Capability Systems Staff**
Director General Maritime Development (Doc Data Sheet only)
Director General Aerospace Development (Doc Data Sheet only)

**Knowledge Staff**

Director General Command, Control, Communications and Computers (DGC4) (Doc Data Sheet only)

Director General Intelligence, Surveillance, Reconnaissance, and Electronic Warfare (DGISREW)R1-3-A142 CANBERRA ACT 2600 (Doc Data Sheet only)

Director General Defence Knowledge Improvement Team (DGDKNIT) R1-5-A165, CANBERRA ACT 2600 (Doc Data Sheet only)

**Army**

ABCA Office, G-1-34, Russell Offices, Canberra (4 copies)

SO (Science), DJFHQ(L), MILPO Enoggera, Queensland 4051 (Doc Data Sheet only)

NAPOC QWG Engineer NBCD c/- DENGRS-A, HQ Engineer Centre Liverpool Military Area, NSW 2174 (Doc Data Sheet only)

**Intelligence Program**

DGSTA Defence Intelligence Organisation

Manager, Information Centre, Defence Intelligence Organisation

**Corporate Support Program**

Library Manager, DLS-Canberra

**UNIVERSITIES AND COLLEGES**

Australian Defence Force Academy

Library

Head of Aerospace and Mechanical Engineering

Serials Section (M list), Deakin University Library, Geelong, 3217

Hargrave Library, Monash University (Doc Data Sheet only)

Librarian, Flinders University

**OTHER ORGANISATIONS**

NASA (Canberra)

AusInfo

**OUTSIDE AUSTRALIA**

**ABSTRACTING AND INFORMATION ORGANISATIONS**

Library, Chemical Abstracts Reference Service

Engineering Societies Library, US

Materials Information, Cambridge Scientific Abstracts, US

Documents Librarian, The Center for Research Libraries, US

**INFORMATION EXCHANGE AGREEMENT PARTNERS**

Acquisitions Unit, Science Reference and Information Service, UK

Library - Exchange Desk, National Institute of Standards and Technology, US

National Aerospace Laboratory, Japan (

National Aerospace Laboratory, Netherlands

SPARES (5 copies)

**Total number of copies:** **45**

**DEFENCE SCIENCE AND TECHNOLOGY ORGANISATION**
**DOCUMENT CONTROL DATA**

1. PRIVACY MARKING/CAVEAT (OF DOCUMENT)

1. TITLE

An Analytically Validated Highly Damped Repair for Acoustically - Induced Cracking on the F/A-18 Nacelle Skin

3. SECURITY CLASSIFICATION (FOR UNCLASSIFIED REPORTS THAT ARE LIMITED RELEASE USE (L) NEXT TO DOCUMENT CLASSIFICATION)

Document (U)
Title (U)
Abstract (U)

2. AUTHOR(S

S. C. Galea and R. J. Callinan

5. CORPORATE AUTHOR

Aeronautical and Maritime Research Laboratory
506 Lorimer St
Fishermans Bend Vic 3207 Australia

| 6a. DSTO NUMBER | 6b. AR NUMBER | 6c. TYPE OF REPORT | 7. DOCUMENT DATE |
|---|---|---|---|
| DSTO-TR-1162 | AR-011-893 | Technical Report | June 2001 |

| 8. FILE NUMBER | 9. TASK NUMBER | 10. TASK SPONSOR | 11. NO. OF PAGES | 12. NO. OF REFERENCES |
|---|---|---|---|---|
| M1/9/518 | 98/192 | DGTA | 36 | 17 |

13. URL on the World Wide Web

http://www.dsto.defence.gov.au/corporate/reports/ DSTO-TR-1162.pdf

14. RELEASE AUTHORITY

Chief, Airframes and Engines Division

15. SECONDARY RELEASE STATEMENT OF THIS DOCUMENT

*Approved for public release*

OVERSEAS ENQUIRIES OUTSIDE STATED LIMITATIONS SHOULD BE REFERRED THROUGH DOCUMENT EXCHANGE, PO BOX 1500, SALISBURY, SA 5108

16. DELIBERATE ANNOUNCEMENT

No Limitations

17. CASUAL ANNOUNCEMENT Yes

18. DEFTEST DESCRIPTORS

Sonic fatigue, viscoelastic damping, power spectra, finite element analysis,constrained layer damping

19. ABSTRACT

The skin of an aircraft can vibrate as a result of pressure waves caused by engine and/or aerodynamic effects. In modern fighter aircraft such as the F/A-18, overall sound pressure levels have been recorded up to 170 dB over the surface of the skin. In the F/A-18, cracking has occurred in the lower nacelle external skin, typically along the boundaries of the panel. These cracks often originate from a fastener line and grow along the boundary and then turn into the centre of the panel. In the case of the F/A-18, cracking was due to higher than expected pressure levels caused by an aerodynamic disturbance at the inlet lip. Initial design of this region was based on an overall sound pressure of 160db, which was based on initial computational fluid dynamics (CFD) work. An attempt was made to repair a panel with a boron fibre patch however this repair did not appear to significantly reduce the crack growth. The design of the repair was based on in-plane loads only. In this report the aim is to develop a patch design, based on a finite element analysis, which significantly reduces crack stress intensity factor for structures subject to intense acoustic environments. A significant reduction in stress intensity is achieved by using a highly-damped patch which incorporates a uni-directional boron/epoxy repair and constrained damping layers which consists of viscoelastic material, which provides the necessary damping, and [0/90] boron/epoxy constraining layers. Such configurations have shown that theoretical reductions in stress intensity factors of up to 10 times are achievable. This has the potential of reducing the mode I stress intensity factor ($K_I$) to the order of $K_I$ threshold thus substantially reducing crack growth.

TECHNICAL REPORT DSTO-TR-1162 AR-011-893 JUNE 2001

DEPARTMENT OF DEFENCE
DEFENCE SCIENCE & TECHNOLOGY ORGANISATION
DSTO

AERONAUTICAL AND MARITIME RESEARCH LABORATORY
506 LORIMER STREET FISHERMANS BEND VICTORIA 3207 AUSTRALIA
TELEPHONE (03) 9626 7000